THE TWO FIXED CENTERS PROBLEM – AN INTEGRABLE HAMILTONIAN SYSTEM

VENKATA SATYA KUMAR, MANEM

The two fixed centers problem — an integrable Hamiltonian system

by

Venkata Satya Kumar, Manem

A thesis submitted to the
School of Graduate Studies
in partial fulfillment of the
requirements for the Degree of
Master of Science in Mathematics

Department of Mathematics and Statistics
Memorial University of Newfoundland

St. John's Newfoundland, Canada August 2009

Abstract

This thesis concerns the dynamical system of the two fixed centers problem restricted to a 2-D case. We use the Hamiltonian approach to find an analytical solution in terms of elliptical coordinates. A detailed analysis of quadratic polynomials whose roots control elliptic integrals involved is discussed. The theory is applied to the analysis of concrete orbits and the predictions of the theory are compared with results of direct numerical integration. We present two applications of the theory. One application is to find the escape velocities of the particle. The second application is to investigate the initial data for the particle to hit one of the fixed masses. The difference between the integrable system with Newtonian potential and a non-integrable system corresponding to the logarithmic potential is presented using the Poincare section technique.

Acknowledgements

It is a pleasure to thank those who made this thesis possible. First and foremost I offer my sincerest gratitude to my supervisor Dr. Sergey Sadov who has supported me throughout my studies with his immense patience and knowledge. I wish to thank my co-supervisor Dr. Chris Radford for his support throughout my program.

I would also like to recognize the School of Graduate Studies and the Department of Mathematics and Statistics for funding my graduate program. Also, I wish to thank all faculty and staff in the Department for their help.

I also take this opportunity to thank all my fellow graduate students for their friendship and support. Good luck to each of you in your future endeavors.

I wholeheartedly thank my family for all the unconditional love, guidance, and encouragement.

Contents

List of Tables

List of Figures

Chapter 1

Introduction

1.1 Historical background

The problem of the motion of a point mass moving under the gravitational influence of two fixed attracting centers was first studied by Euler in the 18th century, in the hope that it would become a useful intermediate step towards the solution of the famous Three Body Problem. Euler, in a series of papers [7, 8, 9], investigated the equations of motion for the two-dimensional (2D) case, i.e. the case where the point mass moves on a plane. The plane is determined by the two attracting centers and the initial position of the point mass; the motion is planar if the initial velocity vector belongs to this plane. Euler introduced elliptical coordinates and showed that the system allows separation of variables. In the 19th century, Jacobi [13] showed that the three-dimensional (3D) case is separable in prolate spheroidal coordinates. Jacobi demonstrated that the system can be integrated using separation of variables, but he did not go through a detailed analysis of possible types of motion, behavior of trajectories and structure of the set of trajectories.

In the early 20th century Charlier [4] has classified various types of trajectories in the planar problem into different classes and sub-classes. The inaccuracies in Charlier's analysis of classification of orbits were earlier noted and corrected by Tallquist

[19]. Recently, Contopoulos and Papadaki [5], identified some more mistakes in Charlier's classification and proved that some of the sub-classes were impossible. Deprit [6] did an exhaustive study of the classification of the trajectories into various classes.

Having studied the integrability of Euler's problem confined to a two-dimensional case, many authors have proceeded to study the integrability in the three-dimensional case. For instance, Erikson and Hill [11] found the third integral of motion in the 3D case (besides the energy and angular momentum about the axis passing through the two fixed centers) explicitly. Generalizing the problem in a different direction, Aksenov, Grebennikov and Demin [1], (See also [2], Ch.2), demonstrated that the problem of motion of a material point in the field of two fixed centers with appropriately chosen complex conjugate masses and imaginary distance between them can be used to develop the analytical theory of motion of a satellite in the gravitational field of a non-spherical planet.

Quantum-mechanical connections have been explored with classical papers as motivation. The quantum problem of ionized hydrogen molecule H_2^+ was first studied by Niessen [14] and Pauli [16]. They classified the orbits and made several energy calculations for various orbits. Related is the work by Strand and Reinhardt [17] on semiclassical quantization of the hydrogen molecule ion.

Interestingly, the two fixed centers problem is encountered as a project in the Applied Mathematics 2130 course at Memorial University under the title of "Cosmic Mini-Golf". The project features an "obstacle star" and a "target black hole". A "planet" is initially placed on the perpendicular bisector to the line connecting the star and the black hole. The goal is to find through numerical analysis different types of trajectories for various initial speeds and angles, and to find the initial values (speed and angle) of the planet such that it hits either the obstacle star or the black hole. One motivation for this thesis was to get more insight regarding the questions posed in the Cosmic Mini-Golf project.

1.2 Outline of this work

We study the two fixed centers problem in a two-dimensional case.

Our approach is different from that used in the recent book written by Ó Mathúna [15]. Ó Mathúna derives the first integral of motion using the Lagrangian method, while we are using the Hamiltonian method. The method of generating function invented by Jacobi [13] is used to describe the coordinate transformation replacing the Cartesian coordinates with elliptic coordinates. We then find integrals of motion that follow from Liouville's theorem.

Another original research done in this thesis is a detailed study of the quadratic polynomials that control the roots of the elliptic integrals, which appear as a result of the separation of variables. Our aim is to apply the theory to the analysis of concrete orbits and to compare predictions of the theory with results of direct numerical integration. The numerical method used throughout the work is Runge-Kutta 4th order method built in Matlab software. We also consider a potential corresponding to the attraction law of inverse first powers, as opposed to Newton's law of inverse squares. Here the potential function is logarithmic. By applying the Poincare section technique, we visualize the difference between an integrable system with Newtonian potential and a non-integrable system with logarithmic potential. We also derive the Erikson-Hill integral for a planar case.

The material of this thesis is organized into six chapters. Chapter 2 introduces the notation and set-up of the model. The later part of this chapter contains the derivation of the Hamiltonian formulation in Cartesian and then in elliptic coordinates. The method of generating function is applied to derive expressions for generalized momenta and thus to complete the canonical transformation to the new variables. In Chapter 3, the resulting Hamiltonian system with two degrees of freedom is transformed into two independent Hamiltonian systems, each with one degree of freedom. To do that, we apply Liouville's theorem. The independent Hamiltonian systems are then integrated to get an analytical solution in terms of elliptic integrals. Chapter 4

presents a detailed analysis of the quadratic polynomials whose roots control the behaviour of elliptic integrals. As a consequence we are able to describe various bounded and unbounded cases of motion and to classify different types of trajectories. We also mention mathematically possible but dynamically forbidden types of trajectories. In Chapter 5, we give two applications of the theory developed before. The first application is to find the escape velocities. The first escape velocity is the minimum velocity the particle should attain to escape from the gravitational influence of the fixed mass that the particle is orbiting. The second escape velocity is the minimum velocity that the particle should attain so that it escapes from the whole system (that is, from the gravitational influence of the two fixed masses). The second application is the collision problem: given the initial position of the particle, we have to find the initial velocity vector so that the particle collides with one of the fixed masses. Chapter 6 is devoted to the numerical study of the integrability of the Hamiltonian system by studying the Poincare section. Our numerical results support theoretical predictions about the integrability of the system with Newtonian potential analyzed in the previous chapters. We compare them with results demonstrating non-integrability of a similar two fixed centers problem with logarithmic potential.

Chapter 2

Planar problem of two fixed centers

2.1 Set-up of the model

This section introduces notations, set-up of the model and the three coordinate systems: Cartesian, polar and elliptic coordinates.

We consider the motion of a particle P in the gravitational field of two fixed bodies. The particle and the two fixed bodies are assumed to be point masses. The problem is two-dimensional. Let (x, y) be the Cartesian coordinates.

The two fixed bodies with masses m_1 and m_2 are placed symmetrically at $x{=}{+}b$ and $x{=}{-}b$ respectively on the x-axis. We will later (starting from the fourth chapter) choose the unit of length so as to make $b = 1$ and the unit of mass so as to make $m_1 + m_2 = 1$.

We are only interested in the motion of the particle P. The mass or even the presence of the particle P has no effect on the fixed masses m_1 and m_2. For these reasons the term reflecting the mass of the particle P will not be included in the potential energy. Since the acceleration of the particle P caused by the two fixed bodies does not depend on its mass, we can assume for convenience that the mass of the particle P is equal to 1.

The particle P is sometimes referred to as the *planet* and the two fixed masses m_1 and m_2 are referred to as the *stars* in the sequel.

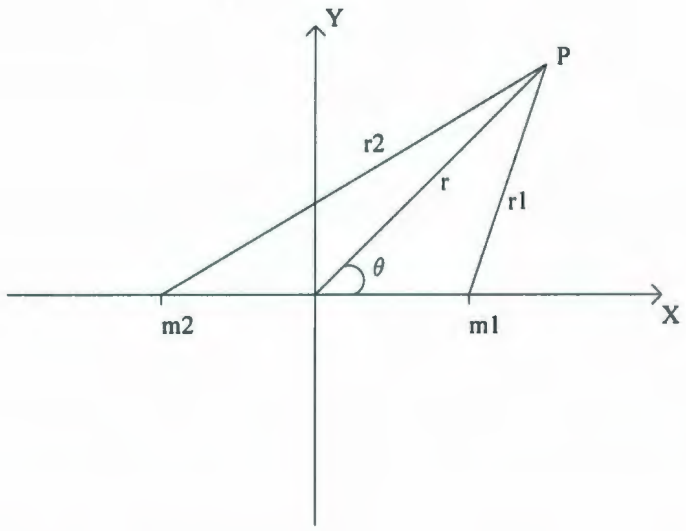

Figure 2.1: A particle P under the gravitational influence of two fixed bodies located at $(b, 0)$ and $(-b, 0)$

The potential energy per unit mass in the gravitational field of the two fixed masses at the point $P(x, y)$ is given by

$$U(x, y) = -G\left(\frac{m_1}{r_1} + \frac{m_2}{r_2}\right), \tag{2.1}$$

where G is the gravitational constant, r_i is the distance from the point P to the fixed mass m_i $(i = 1, 2)$. The negative sign means that the forces are attractive, not repulsive. By choosing the unit of time appropriately we can make $G = 1$, which will be assumed in the sequel. The distances r_1 and r_2 are the functions of x, y given by

$$r_1 = \sqrt{(x-b)^2 + y^2},$$
$$r_2 = \sqrt{(x+b)^2 + y^2}.$$

The equations of motion of the particle P are

$$\ddot{x} = -\frac{dU}{dx}, \quad \ddot{y} = -\frac{dU}{dy}. \tag{2.2}$$

The dot denotes differentiation with respect to the time t.

We will need two more coordinate systems.

First, we introduce the polar coordinates (r, θ) so that

$$x = r\cos\theta,$$
$$y = r\sin\theta.$$

Applying the cosine law we find the expressions for r_1 and r_2 in terms of the polar coordinates

$$\begin{aligned} r_1^2 &= r^2 + b^2 - 2br\cos\theta, \\ r_2^2 &= r^2 + b^2 + 2br\cos\theta. \end{aligned} \tag{2.3}$$

Second, we introduce the elliptic coordinates (R, σ). They will play an important role in the analysis of our dynamical system. The coordinates (R, σ) are defined by the relations

$$\begin{aligned} x &= R\cos\sigma, \\ y &= \sqrt{R^2 - b^2}\,\sin\sigma. \end{aligned} \tag{2.4}$$

As a consequence we have

$$r^2 = x^2 + y^2 = R^2 - b^2\sin^2\sigma. \tag{2.5}$$

We express r_1 and r_2 in terms of R and σ. Using the fact that $r\cos\theta = R\cos\sigma$ and substituting the value of r^2 from (2.5) into (2.3), we obtain

$$\begin{aligned} r_1^2 &= (R^2 - b^2\sin^2\sigma) + b^2 - 2br\cos\theta \\ &= R^2 + b^2\cos^2\sigma - 2bR\cos\sigma. \\ &= (R - b\cos\sigma)^2. \end{aligned}$$

Also

$$\begin{aligned} r_2^2 &= (R^2 - b^2\sin^2\sigma) + b^2 + 2br\cos\theta \\ &= R^2 + b^2\cos^2\sigma + 2bR\cos\sigma. \\ &= (R + b\cos\sigma)^2. \end{aligned}$$

Therefore, r_1 and r_2 in terms of R and σ are

$$\begin{aligned} r_1 &= R - b\cos\sigma, \\ r_2 &= R + b\cos\sigma. \end{aligned} \tag{2.6}$$

2.2 Level curves of elliptic coordinates R and σ

In this section we find level curves (in other words, grid lines) of the elliptic coordinates R and σ.

We first find the level curves of R. From equations (2.4) we have

$$\cos\sigma = \frac{x}{R}, \quad \sin\sigma = \frac{y}{\sqrt{R^2 - b^2}}. \tag{2.7}$$

Let $R = \rho b$. We fix ρ and let σ vary. Combining the equations (2.7), we get

$$\frac{x^2}{\rho^2} + \frac{y^2}{\rho^2 - 1} = 1,$$

which is an equation of an ellipse with eccentricity

$$e = \sqrt{1 - \frac{\rho^2 - 1}{\rho^2}} = \frac{1}{\rho}.$$

All these ellipses have common foci at $(\rho, \sigma) = (\pm 1, 0)$, equivalently, $(R, \sigma) = (\pm b, 0)$.

Let us mention two special cases.

1. Let us suppose that $R \longrightarrow b$, or, equivalently, $\rho \longrightarrow 1$. Then

$$\begin{aligned} x &\approx b\cos\sigma, \\ y &\approx 0. \end{aligned}$$

Since $\cos\sigma$ lies between -1 and $+1$, the values that x can take are between $-b$ and $+b$. Hence the points of the major axis of the ellipse lie between $(-b, 0)$ and $(b, 0)$ the ellipse becomes an interval which is shown in Figure 2.2.

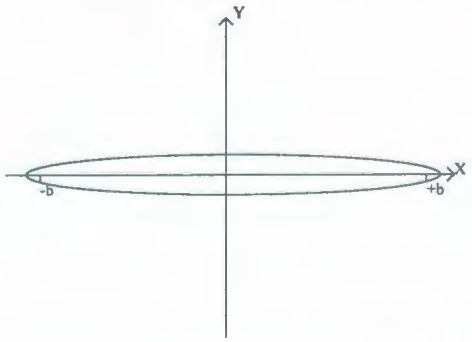

Figure 2.2: The level curve of R in the limiting case of an interval ($R \to b^+$)

2. Let us suppose that R is much greater than b.

   The level curve is then approximately a circle, which is one of the limiting cases of an ellipse, which is shown in Figure 2.3.

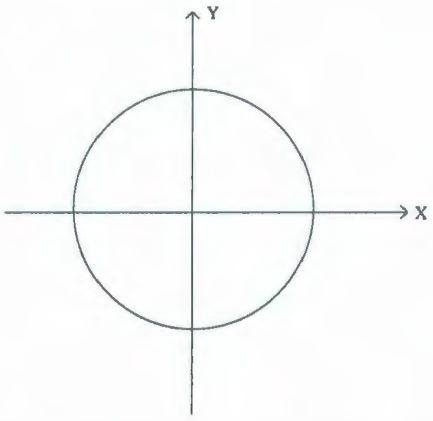

Figure 2.3: The level curve of R in the limiting case of a circle ($R \to \infty$)

Now we find the level curves of σ.

From equations (2.4) we have

$$\cos\sigma = \frac{x}{R}, \quad \sin\sigma = \frac{y}{\sqrt{R^2 - b^2}}. \tag{2.8}$$

Combining the above equations, we get

$$\frac{x^2}{\cos^2\sigma} - \frac{y^2}{\sin^2\sigma} = -b^2,$$

which is an equation of an hyperbola. All these hyperbolas have common foci at $(\pm b, 0)$. To find the asymptotes of the hyperbola, we assume that x and y are large. Then

$$\frac{x^2}{\cos^2\sigma} - \frac{y^2}{\sin^2\sigma} \approx 0. \tag{2.9}$$

Hence, equations of the asymptotes are $y = \pm x\tan\sigma$. Two special cases are the following.

1. For σ=0 or σ=π, the corresponding values are x=$\pm R$ and y=0.

   Therefore the points on the hyperbola are of the form $(x, y) = (\pm R, 0)$, where

$R \in [1, \infty)$. The hyperbola folds on two rays as shown in Figure 2.4.

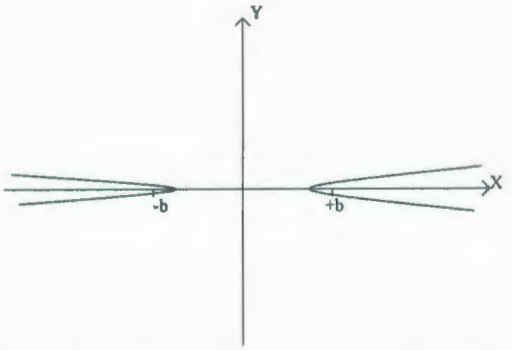

Figure 2.4: The level curve of $\sigma \approx 0$ or π is a hyperbola with its vertices near $(\pm 1, 0)$ and its asymptotes extending to ∞ along the x axis

2. For $\sigma = \frac{\pi}{2}$ and $\sigma = \frac{3\pi}{2}$, the corresponding values are $x=0$ and $y = \pm\sqrt{R^2 - b^2}$, $|R| \geq b$. The hyperbola becomes a double line $x = 0$. The corresponding plot is shown in Figure 2.5.

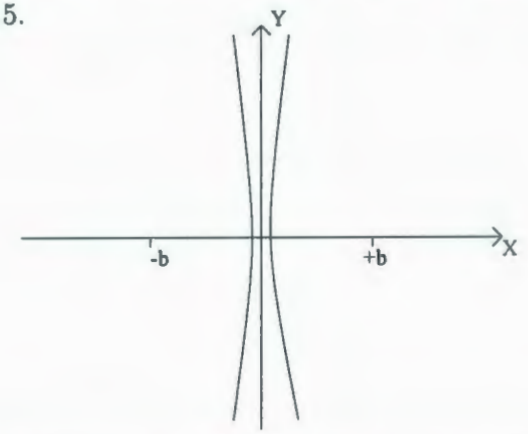

Figure 2.5: The level curve of $\sigma \approx \frac{\pi}{2}, \frac{3\pi}{2}$ is an hyperbola with its vertices near $(0, 0)$ and with its asymptotes extending to ∞ along the y axis

2.3 Hamiltonian formulation in Cartesian and in elliptic coordinates

This section contains the derivation of the Hamiltonian formulation in the Cartesian coordinates and then in the elliptic coordinates. The method of generating function is applied to derive the generalized momenta.

We use the Hamiltonian approach to replace the system (2.2) of two ordinary differential equations (ODE) of the 2nd order by a system of four ODE's of the 1st order of a special, Hamiltonian, form. A Hamiltonian system is determined by Hamilton's function, or the Hamiltonian. The Hamiltonian H represents the total energy of the system

$$H = T + U,$$

which is the sum of the potential energy U and the kinetic energy T.

In our case, U is defined by (2.1) and the kinetic energy is

$$T(p_x, p_y) = \frac{1}{2}(p_x^2 + p_y^2). \tag{2.10}$$

Here p_x and p_y are the components of the momentum of the particle P. Since we have assumed that the mass of the particle is 1, we have

$$p_x = \dot{x}, \qquad p_y = \dot{y}.$$

Thus the Hamiltonian is a function of four variables x, y, p_x, p_y, which are called the phase variables:

$$H(x, y, p_x, p_y) = \frac{1}{2}(p_x^2 + p_y^2) - \frac{m_1}{r_1} - \frac{m_2}{r_2}. \tag{2.11}$$

As known from the Hamiltonian mechanics, the equations of motion (2.2) can be written in the Hamiltonian form

$$\begin{aligned} \dot{x} &= \frac{\partial H}{\partial p_x}, & \dot{p}_x &= -\frac{\partial H}{\partial x}, \\ \dot{y} &= \frac{\partial H}{\partial p_y}, & \dot{p}_y &= -\frac{\partial H}{\partial y}. \end{aligned} \tag{2.12}$$

We have a Hamiltonian system with two degrees of freedom. It is known that such systems in general are not solvable analytically, i.e. the solution cannot be expressed in terms of integrals involving coordinates, time and other system's parameters. The dynamical system which we have set up is not general in that sense. In the end, we will be able to conclude that the system (2.12) is analytically integrable. An analytical solution will be obtained by using the elliptical coordinates (R, σ).

The advantage of using the Hamiltonian approach is that it is more universal and we can write our system in an equivalent Hamiltonian form with respect to different coordinate systems.

The Hamiltonian function (with two degrees of freedom) in general depends on four phase variables, of which two are considered to be generalized coordinates and the other two are generalized momenta. The generalized coordinates can be chosen more or less arbitrarily as functions of the original coordinates and momenta. The generalized momenta are then determined rigidly because of the very special structure of the Hamiltonian equations.

In our case we choose the elliptic coordinates (R, σ) as the generalized coordinates. To find the corresponding momenta we use the method of generating function invented by C.G. Jacobi [13].

We need to find a generating function $S(R, \sigma, p_x, p_y)$, from which the new momenta will be obtained as

$$p_R = \frac{\partial S}{\partial R}, \quad p_\sigma = \frac{\partial S}{\partial \sigma}. \tag{2.13}$$

The generating function S is constructed as a solution of a system of partial differential equations

$$\frac{\partial S}{\partial p_x} = x(R, \sigma), \quad \frac{\partial S}{\partial p_y} = y(R, \sigma). \tag{2.14}$$

According to the relations (2.4), we can rewrite the system as follows:

$$\begin{aligned} \frac{\partial S}{\partial p_x} &= R\cos\sigma, \\ \frac{\partial S}{\partial p_y} &= \sqrt{R^2 - b^2}\sin\sigma. \end{aligned} \tag{2.15}$$

Any particular solution is suitable for our purpose. A simple particular solution is given by

$$S = p_x R\cos\sigma + p_y\sqrt{R^2-b^2}\,\sin\sigma. \tag{2.16}$$

Therefore, the new momenta are

$$\begin{aligned} p_R &= \frac{\partial S}{\partial R} \\ &= p_x\cos\sigma + p_y\frac{R\sin\sigma}{\sqrt{R^2-b^2}} \end{aligned} \tag{2.17}$$

and

$$\begin{aligned} p_\sigma &= \frac{\partial S}{\partial \sigma} \\ &= -p_x R\sin\sigma + p_y\sqrt{R^2-b^2}\,\cos\sigma. \end{aligned} \tag{2.18}$$

Notice that p_R and p_σ are linear functions in p_x and p_y. Therefore we can write the above system in a matrix form

$$\begin{bmatrix} p_R \\ p_\sigma \end{bmatrix} = M \begin{bmatrix} p_x \\ p_y \end{bmatrix},$$

where

$$M = \begin{bmatrix} \cos\sigma & \dfrac{R\sin\sigma}{\sqrt{R^2-b^2}} \\ -R\sin\sigma & \sqrt{R^2-b^2}\cos\sigma \end{bmatrix}.$$

By the matrix inversion formula we find p_x and p_y in terms of p_R and p_σ:

$$\begin{bmatrix} p_x \\ p_y \end{bmatrix} = \frac{1}{\det M}\begin{bmatrix} \sqrt{R^2-b^2}\,\cos\sigma & \dfrac{-R\sin\sigma}{\sqrt{R^2-b^2}} \\ R\sin\sigma & \cos\sigma \end{bmatrix}\begin{bmatrix} p_R \\ p_\sigma \end{bmatrix}, \tag{2.19}$$

where

$$\det M = \frac{-b^2\cos^2\sigma + R^2}{\sqrt{R^2-b^2}}.$$

We now calculate the kinetic energy (2.10) in terms of R and σ:

$$\begin{aligned} T &= \frac{1}{2}\left[p_x^2 + p_y^2\right] \\ &= \frac{1}{2}\left[\left(p_R\sqrt{R^2-b^2}\cos\sigma - \frac{p_\sigma R\sin\sigma}{\sqrt{R^2-b^2}}\right)^2 + (p_R R\sin\sigma + p_\sigma\cos\sigma)^2\right] \\ &\quad \times\frac{R^2-b^2}{(-b^2\cos^2\sigma+R^2)^2} \\ &= \frac{1}{2}\left[\frac{(R^2-b^2)p_R^2}{(R^2-b^2\cos^2\sigma)} + \frac{p_\sigma^2}{(R^2-b^2\cos^2\sigma)}\right]. \end{aligned}$$

Therefore the kinetic energy is

$$T(R,\sigma,p_R,p_\sigma) = \frac{1}{2}\left[\frac{(R^2-b^2)p_R^2}{(R^2-b^2\cos^2\sigma)} + \frac{p_\sigma^2}{(R^2-b^2\cos^2\sigma)}\right]. \tag{2.20}$$

According to (2.1) and (2.6), the potential energy is

$$\begin{aligned} U(R,\sigma) &= -\left(\frac{m_1}{r_1} + \frac{m_2}{r_2}\right) \\ &= -\left(\frac{m_1}{R-b\cos\sigma} + \frac{m_2}{R+b\cos\sigma}\right). \end{aligned} \tag{2.21}$$

Therefore, the Hamiltonian in terms of (R,σ) is

$$H = \frac{(R^2-b^2)p_R^2 + p_\sigma^2}{2(R^2-b^2\cos^2\sigma)} - \left[\frac{m_1}{R-b\cos\sigma} + \frac{m_2}{R+b\cos\sigma}\right]. \tag{2.22}$$

A transformation generated by the function S satisfying the equations (2.14), (2.15) is called a canonical transformation. The equations (2.12) in the new variables (R,σ,p_R,p_σ) again have a Hamiltonian form

$$\begin{aligned} \dot{R} &= \frac{\partial H}{\partial p_R}, \qquad & \dot{p}_R &= -\frac{\partial H}{\partial R}, \\ \dot{\sigma} &= \frac{\partial H}{\partial p_\sigma}, \qquad & \dot{p}_\sigma &= -\frac{\partial H}{\partial \sigma}. \end{aligned} \tag{2.23}$$

At first sight it's not clear why the system (2.23) is any better than the system (2.12). The only fact that we can state now is that both systems have an integral of motion

$$H = E,$$

where E is the energy of the system (a number), while H in the left hand side is a function of the phase variables. Thus the motion in the dynamical system (2.23) occurs along trajectories that lie on energy surfaces

$$H(R, \sigma, p_R, p_\sigma) = E. \tag{2.24}$$

If we can find a second integral, independent of H, in a dynamical system with two degrees of freedom, then the system can be integrated. This is rarely possible. However, a Hamiltonian system with one degree of freedom has energy as its integral and this is sufficient to determine the trajectories of the system.

Moreover, in any system of two first order ODE's

$$\dot{p} = f(p, q), \quad \dot{q} = g(p, q) \tag{2.25}$$

the knowledge of an integral $F(p, q) = A$ allows one to determine the trajectories of the system. We solve this equation for one of the variables, say p, in terms of the other variable, say q. We then substitute the function $p(A, q)$ into the equation $\dot{q} = g(p, q)$. The position of the particle on the trajectory at a given time t can be found by integrating the equation

$$dt = \frac{dq}{g(p(A, q), q)}.$$

In the right hand side we have a function in one variable q, which we integrate and obtain $t(q)$, which also depends on the parameter A.

The trajectories of the system (2.25) are in fact the same as the trajectories of the Hamiltonian system with the Hamiltonian $F(p, q)$:

$$\frac{dp}{d\tau} = \frac{dF}{dq}, \quad \frac{dq}{d\tau} = -\frac{dF}{dp}. \tag{2.26}$$

However, the new time variable τ is not identical to t.

The reduction of the Hamiltonian system (2.23) to a pair of independent Hamiltonian systems of the type (2.26) is carried out in the subsequent chapter.

Chapter 3

Complete integrability of the problem

3.1 Separation of variables

In this section we apply Liouville's theorem to transform the Hamiltonian system with two degrees of freedom into two independent Hamiltonian systems, each with one degree of freedom.

Denote

$$Q(R,\sigma) = R^2 - b^2\cos^2\sigma. \tag{3.1}$$

Multiplying equation (2.24) by $Q(R,\sigma)$ and using (2.22), we get

$$\left[p_R^2(R^2-b^2)+p_\sigma^2\right] - 2\left[m_1(R+b\cos\sigma)+m_2(R-b\cos\sigma)\right] = 2EQ(R,\sigma).$$

We rearrange the terms by placing those depending on R and p_R on one side, and those depending on σ and p_σ on the other side:

$$p_R^2(R^2-b^2) - 2R(m_1+m_2) - 2ER^2 = -2Eb^2\cos^2\sigma - p_\sigma^2 + 2b(m_1-m_2)\cos\sigma. \tag{3.2}$$

Suppose for a moment that this equation holds identically in the entire space $\mathbb{R}^4$ with coordinates (R,σ,p_R,p_σ). Since the two sides of equation (3.2) depend on two

different pairs of variables, they have to be equal to a common constant, which we denote as A. Let us introduce the independent Hamiltonian functions

$$H_1(R, p_R) = p_R^2(R^2 - b^2) - 2R(m_1 + m_2) - 2ER^2 \tag{3.3}$$

and

$$H_2(\sigma, p_\sigma) = -2Eb^2 \cos^2\sigma - p_\sigma^2 - 2b(m_2 - m_1)\cos\sigma. \tag{3.4}$$

Equation (3.2) can now be written as a system of two equations with an auxiliary constant A:

$$H_1(R, p_R) = A, \tag{3.5}$$

$$H_2(\sigma, p_\sigma) = A. \tag{3.6}$$

The constant A does not have a direct physical meaning by itself, but it is related to the angular momenta of the particle with respect to the fixed masses, as we will explain in Section 3.3.

The Hamiltonian system determined by the Hamiltonian (3.3) is

$$\begin{aligned} \frac{dR}{d\tau} &= \frac{\partial H_1}{\partial p_R} &&= 2p_R(R^2 - b^2), \\ \frac{dp_R}{d\tau} &= -\frac{\partial H_1}{\partial R} &&= -\left[2Rp_R^2 - 2(m_1 + m_2) - 4ER\right]. \end{aligned} \tag{3.7}$$

The Hamiltonian system determined by the Hamiltonian (3.4) is

$$\begin{aligned} \frac{d\sigma}{d\tau} &= \frac{\partial H_2}{\partial p_\sigma} &&= -2p_\sigma, \\ \frac{dp_\sigma}{d\tau} &= -\frac{\partial H_2}{\partial \sigma} &&= -(4Eb^2 \cos\sigma \sin\sigma + 2b(m_2 - m_1)\sin\sigma) \\ & && = -2Eb^2 \sin 2\sigma + 2b(m_1 - m_2)\sin\sigma. \end{aligned} \tag{3.8}$$

Thus, if indeed the equations (3.5) and (3.6) hold, then we have obtained two independent Hamiltonian systems for the two groups of variables (R, p_R) and (σ, p_σ).

However, we cannot claim in advance that the right hand side A in the equations (3.5) and (3.6) is a constant. This is because the equation (3.2), i.e. $H_1(R, p_R) =$

$H_2(\sigma, p_\sigma)$, holds only on the energy surface and not in the whole four-dimensional phase space, i.e. E in (3.3) and (3.4) is constant only on the energy surface. (For example, the equation $x^2 = 1-y^2$ holds on the unit circle and it does not imply that x is a constant and y is a constant.) However, we can still make a connection between the solutions of the systems (3.7) and (3.8) with the solution of the Hamiltonian system (2.23). This connection is a particular case of Liouville's theorem that follows.

Let us generalize the situation. Let $H(q_1, p_1, q_2, p_2)$ be a Hamiltonian function of the form

$$H(q_1, p_1, q_2, p_2) = \frac{1}{Q(q_1, q_2)}(F_1(q_1, p_1) + F_2(q_2, p_2)). \tag{3.9}$$

with

$$Q(q_1, q_2) = Q_1(q_1) + Q_2(q_2). \tag{3.10}$$

Consider the energy surface $H = E$. Multiplying this equation by Q, we get

$$F_1(q_1, p_1) + F_2(q_2, p_2) = EQ(q_1, q_2).$$

Substituting (3.10), we obtain

$$(F_1(q_1, p_1) - EQ_1(q_1)) + (F_2(q_2, p_2) - EQ_2(q_2)) = 0. \tag{3.11}$$

Let us denote

$$H_1(q_1, p_1) = F_1(q_1, p_1) - EQ_1(q_1) \tag{3.12}$$

and

$$H_2(q_2, p_2) = -F_2(q_2, p_2) + EQ_2(q_2). \tag{3.13}$$

If the equation (3.11) were true in the entire space, then we could conclude that $H_1 = A$ and $H_2 = A$ with a constant A. The actual situation is not so simple but the separation of variables is nevertheless possible due to Liouville's theorem, which we'll now prove.

Theorem. *Suppose $q_1(\tau)$, $p_1(\tau)$ is a solution of the system with Hamiltonian (3.12) and $q_2(\tau)$, $p_2(\tau)$ is a solution of the system with Hamiltonian (3.13), that is,*

$$\frac{dq_1}{d\tau} = \frac{\partial H_1}{\partial p_1}, \qquad \frac{dp_1}{d\tau} = -\frac{\partial H_1}{\partial q_1}; \tag{3.14}$$

$$\frac{dq_2}{d\tau} = \frac{\partial H_2}{\partial p_2}, \qquad \frac{dp_2}{d\tau} = -\frac{\partial H_2}{\partial q_2}. \tag{3.15}$$

Suppose also that a new time variable $t(\tau)$ is defined by

$$\frac{dt}{d\tau} = Q(q_1(\tau), q_2(\tau)). \tag{3.16}$$

Let dot represent the derivative with respect to t. Then

$$\dot{q}_1 = \frac{\partial H}{\partial p_1}, \qquad \dot{q}_2 = \frac{\partial H}{\partial p_2}, \tag{3.17}$$

and

$$\dot{p}_1 = -\frac{\partial H}{\partial q_1}, \qquad \dot{p}_2 = -\frac{\partial H}{\partial q_2}, \tag{3.18}$$

So $(q_1(t), q_2(t), p_1(t), p_2(t))$ is a solution of the Hamiltonian system with Hamiltonian (3.9).

Proof. Let us consider

$$\begin{aligned} \dot{q}_1 &= \frac{dq_1}{d\tau}\frac{d\tau}{dt} \\ &= \frac{\partial H_1}{\partial p_1}\frac{1}{Q(q_1, q_2)} \\ &= \frac{\partial F_1}{\partial p_1}\frac{1}{Q(q_1, q_2)}, \end{aligned} \tag{3.19}$$

by equation (3.12). When we differentiate the Hamiltonian (3.12), we treat E as a constant. But from equation (3.9) we have

$$\frac{\partial H}{\partial p_1} = \frac{1}{Q(q_1, q_2)}\frac{\partial F_1}{\partial p_1}. \tag{3.20}$$

Comparing equations (3.19) and (3.20), we conclude that

$$\dot{q}_1 = \frac{\partial H_1}{\partial p_1}.$$

Next, we consider

$$\begin{aligned} \dot{p}_1 &= \frac{dp_1}{d\tau}\frac{d\tau}{dt} \\ &= -\frac{\partial H_1}{\partial q_1}\frac{1}{Q} \\ &= -(\frac{\partial F_1}{\partial q_1} - E\frac{\partial Q_1}{\partial q_1})\frac{1}{Q} \\ &= -\frac{1}{Q}\frac{\partial F_1}{\partial q_1} + E\frac{1}{Q}\frac{\partial Q_1}{\partial q_1}. \end{aligned} \tag{3.21}$$

Differentiating equation (3.9) with respect to q_1, we get

$$\frac{\partial H}{\partial q_1} = \frac{1}{Q}\frac{\partial F_1}{\partial q_1} - \frac{\partial Q_1}{\partial q_1}\frac{F_1 + F_2}{Q^2}.$$

Using equation (3.9) again, we replace $\frac{F_1 + F_2}{Q}$ by H. Also, $H = E$ on the energy surface. So, replacing H by E in the above equation, we obtain

$$-\frac{\partial H}{\partial q_1} = -\frac{1}{Q}\frac{\partial F_1}{\partial q_1} + \frac{\partial Q_1}{\partial q_1}\frac{E}{Q}. \tag{3.22}$$

From equations (3.21) and (3.22) we conclude that

$$\dot{p}_1 = -\frac{\partial H_1}{\partial q_1}.$$

The proof of the equations for $\dot{q}_2$ and $\dot{p}_2$ is analogous. Hence the theorem. □

We apply the above theorem in our model to obtain the two independent dynamical systems. The correspondence between the variables and the functions in Liouville's theorem, on the one hand, and in our model on the other hand, is shown in Table 3.1.

Table 3.1: Correspondence between Liouville's theorem and our model

Theorem	Our model
$F_1(p_1, q_1)$	$p_R^2(R^2 - b^2) - 2m_1R - 2m_2R$
$F_2(p_2, q_2)$	$p_\sigma^2 + 2m_2 b\cos\sigma - 2m_1 b\cos\sigma$
$Q_1(q_1)$	R^2
$Q_2(q_2)$	$-b^2\cos^2\sigma$

3.2 Two Hamiltonian systems with one degree of freedom

In this section the independent Hamiltonian systems obtained in the previous section are integrated to get an analytical solution in terms of elliptic integrals.

Fix the value of the constant A in (3.5) and (3.6).

Let us consider the Hamiltonian function (3.3). By the equation (3.5)

$$p_R^2(R^2 - b^2) = A + 2R(m_1 + m_2) + 2ER^2,$$

We have

$$\pm p_R = \sqrt{\frac{A + 2R(m_1 + m_2) + 2ER^2}{R^2 - b^2}}. \tag{3.23}$$

Substituting into the first equation of (3.7), we get

$$\begin{aligned} \frac{dR}{d\tau} = \frac{\partial H_1}{\partial p_R} &= \pm 2\sqrt{\frac{A + 2R(m_1 + m_2) + 2ER^2}{R^2 - b^2}}(R^2 - b^2) \\ &= \pm 2\sqrt{(A + 2R(m_1 + m_2) + 2ER^2)(R^2 - b^2)}. \end{aligned}$$

Hence

$$\frac{dR}{\sqrt{(A + 2R(m_1 + m_2) + 2ER^2)(R^2 - b^2)}} = \pm 2\, d\tau. \tag{3.24}$$

Integration of this equation yields $\tau(R)$ as an elliptic integral and the inverse function gives a solution $R(\tau)$. Then we can find $p_R(\tau)$ using equation (3.23).

The Hamiltonian system with Hamiltonian $H_2(\sigma, p_\sigma)$ is integrated similarly.

From equations (3.4) and (3.6) we have

$$\pm p_\sigma = \sqrt{-2Eb^2\cos^2\sigma - 2b\cos\sigma(m_2 - m_1) - A}. \tag{3.25}$$

Substituting in the first equation of (3.8), we get

$$\frac{d\sigma}{\sqrt{-2Eb^2\cos^2\sigma - 2b\cos\sigma(m_2 - m_1) - A}} = \mp 2\, d\tau. \tag{3.26}$$

We use a change of variable in order to obtain an algebraic function similar to that in (3.24) instead of a trigonometric function in the denominator of the above equation.

For this purpose let $\cos\sigma = S$, then $\sin\sigma = \sqrt{1 - S^2}$ and $dS = -\sin\sigma\, d\sigma$. Substituting in (3.26), we get

$$\frac{dS}{\sqrt{(1 - S^2)(-2Eb^2S^2 - 2bS(m_2 - m_1) - A)}} = \pm 2\, d\tau. \tag{3.27}$$

Integration of this equation yields $\tau(S)$ as an elliptic integral and the inverse function gives a solution $S(\tau)$. Then we can find $\sigma(\tau)$ and $p_\sigma(\tau)$ using equation (3.25).

Introduce the notation $\rho = \dfrac{R}{b}$ and the polynomials

$$G(\rho) = 2Eb^2\rho^2 + 2b\rho(m_1 + m_2) + A, \tag{3.28}$$

$$F(S) = -2Eb^2S^2 - 2bS(m_2 - m_1) - A, \tag{3.29}$$

which will enable us to write the equations (3.24) and (3.26) in a shorter form. The sign of these polynomials $F(S)$ and $G(\rho)$ is going to be very important in the subsequent chapters. Their coefficients define the parametric space of possible solutions of our problem.

Substituting $R = b\rho$ in (3.24) gives

$$\frac{d\rho}{\sqrt{(\rho^2-1)(A + 2b\rho(m_1+m_2) + 2Eb^2\rho^2))}} = \pm 2\, d\tau. \tag{3.30}$$

Therefore

$$\frac{d\rho}{\sqrt{(\rho^2-1)G(\rho)}} = \pm 2\, d\tau. \tag{3.31}$$

Also from (3.26) and (3.29) we get

$$\frac{dS}{\sqrt{(1-S^2)F(S)}} = \pm 2\, d\tau. \tag{3.32}$$

The variable S in (3.32) is subject to constraint

$$-1 \le S \le 1, \tag{3.33}$$

because $S = \cos\sigma$.

The variable ρ in (3.31) is subject to constraint

$$\rho \ge 1, \tag{3.34}$$

because of the second equation in (2.4).

Elliptic integrals and their inverses — elliptic functions — are commonly studied by means of complex analysis. In this thesis, we will use only a few formulas from the theory of elliptic functions. We manipulate them with the help of Maple software.

3.3 The Erikson-Hill integral

This section gives some idea about a physical meaning of the auxiliary constant A which we introduced in equations (3.5) and (3.6) of the previous section. Here we provide a detailed derivation, not found in the literature, of the Erikson-Hill integral [11] in the planar case.

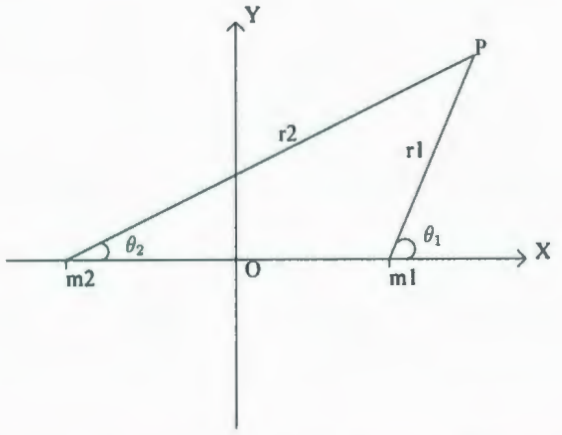

Figure 3.1: Angles θ_1, θ_2 in the Erikson-Hill integral

Let θ_1 and θ_2 be the angles shown in Figure (3.1). According to (2.4) we have

$$\cos\theta_1 = \frac{x-b}{r_1} = \frac{R\cos\sigma - b}{R - b\cos\sigma},$$

$$\cos\theta_2 = \frac{x+b}{r_2} = \frac{R\cos\sigma + b}{R + b\cos\sigma}.$$

Theorem. *Suppose L_1 and L_2 are the angular momenta of the particle relative to the two fixed masses m_1 and m_2. Then the following quantity is an integral of motion:*

$$\Omega = L_1 L_2 - 2b(m_1\cos\theta_1 - m_2\cos\theta_2). \tag{3.35}$$

The relation between Ω, the Hamiltonian H (2.22) and the two auxilariary Hamiltonians H_1 and H_2 given by (3.3) and (3.4) is

$$\Omega = -2b^2 H + c_1 H_1 + c_2 H_2, \tag{3.36}$$

where c_1 and c_2 are any two constants such that $c_1 + c_2 = -1$.

Proof:

The angular momentum of the particle P relative to the mass m_1 is

$$\begin{aligned} L_1 &= \begin{vmatrix} p_x & x-b \\ p_y & y \end{vmatrix} \\ &= yp_x - (x-b)p_y. \end{aligned}$$

Substituting (2.4) and (2.15), we obtain

$$L_1 = \frac{\sqrt{R^2-b^2}}{Q}(R - b\cos\sigma)(p_R b\sin\sigma - p_\sigma). \tag{3.37}$$

To find an expression for L_2, we replace b by $-b$ and get

$$L_2 = \frac{\sqrt{R^2-b^2}}{Q}(R + b\cos\sigma)(-p_R b\sin\sigma - p_\sigma). \tag{3.38}$$

Thus by (3.1) we have

$$L_1 L_2 = \frac{R^2-b^2}{Q}(p_\sigma^2 - b^2 p_R^2 \sin^2\sigma). \tag{3.39}$$

The expression for Ω as defined by (3.35) becomes

$$\Omega = \frac{(R^2-b^2)}{Q}(p_\sigma^2 - b^2 p_R^2\sin^2\sigma) - 2b\left(\frac{m_1(R\cos\sigma - b)}{R - b\cos\sigma} - \frac{m_2(R\cos\sigma + b)}{R + b\cos\sigma}\right). \tag{3.40}$$

We will show that there exist constants c_0, c_1, c_2 such that

$$\Omega = c_0 H + c_1 H_1 + c_2 H_2. \tag{3.41}$$

Let us compare the coefficients of m_1 in the left and right sides of (3.41).

The coefficient of m_1 in the expression for Ω is $\dfrac{-2b(R\cos\sigma - b)}{R - b\cos\sigma}$.

By (2.22), (3.3), (3.4) the coefficient of m_1 in the expression $(c_0 H + c_1 H_1 + c_2 H_2)$ is $\dfrac{-c_0 + 2b\cos\sigma(c_1 + c_2)}{R - b\cos\sigma}$.

(We have replaced E in the expressions (3.3) and (3.4) with H). Now, comparing the coefficients of m_1 from the above expressions, we obtain

$$c_0 = -2b^2, \quad c_1 + c_2 = -1. \tag{3.42}$$

The same relations are obtained when we compare the coefficients of m_2.

We now compare the coefficients of p_R^2 in the left and right sides of (3.41).

The coefficient of p_R^2 in the expression for Ω is $\dfrac{-(R^2 - b^2)b^2 \sin^2 \sigma}{Q}$.

The coefficient of p_R^2 in the expression $(c_0 H + c_1 H_1 + c_2 H_2)$ is

$$\frac{R^2 - b^2}{Q}\left[\frac{c_0}{2} - b^2(c_1 + c_2) + b^2 \sin^2 \sigma (c_1 + c_2)\right].$$

Now, comparing the coefficients of p_R^2 from the above expressions, we obtain the same relations as in (3.42).

Finally we compare the coefficients of p_σ^2 in the left and right sides of (3.41).

The coefficient of p_σ^2 in the expression for Ω is $\dfrac{(R^2 - b^2)}{Q}$.

The coefficient of p_σ^2 in the expression $(c_0 H + c_1 H_1 + c_2 H_2)$ is $\dfrac{c_0 - 2R^2(c_1 + c_2)}{2Q}$.

Again, comparing the coefficients of p_σ^2 from the above expressions we obtain the same relations as in (3.42).

Therefore the relations (3.42) are necessary and sufficient for (3.41) to hold.

Since H, H_1, H_2 are integrals, so (3.35) is an integral. □

Chapter 4

Analysis of quadratic polynomials and classification of trajectories

4.1 Analysis of the polynomial $F(S)$

Sections 4.1 and 4.2 describe the analysis of the polynomials (3.28) and (3.29), which were derived from the individual Hamiltonian systems (3.7) and (3.8) and whose roots control the behaviour of the elliptic integrals.

From now on, we set b=1. Thus $\rho = \dfrac{R}{b} = R$. We denote

$$2E = \varepsilon, \quad m_2 - m_1 = \beta.$$

and we let $\beta = 0.1$ throughout our analysis. For $0 < \beta < 1$ one would observe a similar qualitative picture. For $\beta = 0$ the configuration is symmetric and some formulas are simplified, but this case is not analyzed here; the additional symmetry makes it qualitatively different (see [15], Section 6, Chapter 3).

We choose the unit of mass so that

$$m_1 + m_2 = 1.$$

The expressions (3.28) and (3.29) are simplified to

$$G(\rho) = \varepsilon\rho^2 + 2\rho + A, \tag{4.1}$$

$$F(S) = -\varepsilon S^2 - 2\beta S - A. \tag{4.2}$$

We investigate the parametric space by plotting separating lines that cut the A-ε plane into different regions. Then we analyze each of the regions individually.

The separating lines for the equation $F(S) = -\varepsilon S^2 - 2\beta S - A = 0$ separate regions with different number of roots on the "good" interval $[-1, 1]$.

These lines are:

1. The A-axis ($\varepsilon = 0$);
2. The discriminant $D = 0$:
$$\varepsilon = \frac{(2\beta)^2}{4A}; \tag{4.3}$$
3. One of the roots is -1:
$$-\varepsilon + 2\beta - A = 0. \tag{4.4}$$
4. One of the roots is $+1$:
$$-\varepsilon - 2\beta - A = 0. \tag{4.5}$$

Figure 4.1 presents the plot of the separating lines.

In Figure 4.1, the hyperbola corresponds to the separating line (4.3); the line passing through the first quadrant corresponds to the separating line (4.4); the line passing through the third quadrant corresponds to the separating line (4.5). The separating lines divide the parametric space A-ε into different regions denoted by roman numerals (I) to (X).

The graphs below show schematically the position of the real roots of the polynomial $F(S)$ relative to the interval $[-1, 1]$ in the cases corresponding to different regions as shown in Figure 4.1.

- Region I: In this region $\varepsilon < 0$. The leading coefficient in $F(S)$ is positive, hence the parabola is opening upwards. Also, $F(-1) < 0$ and $F(1) < 0$. The two roots lie outside the interval $[-1, 1]$ which is shown in Figure 4.2.

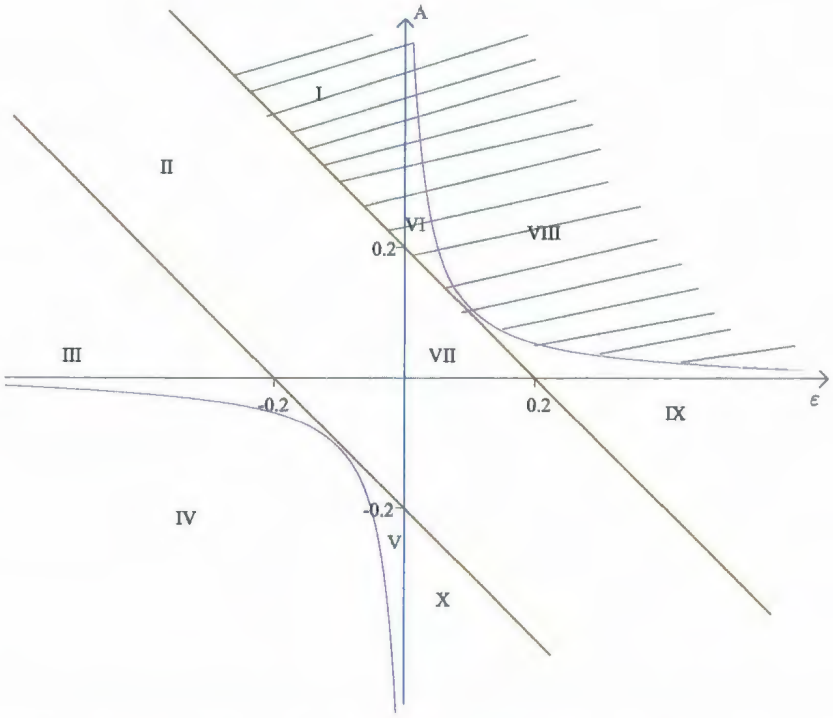

Figure 4.1: Separating lines for $F(S)$. The line passing through first quadrant corresponds to $F(-1)$=0; the line passing through third quadrant corresponds to $F(+1)$=0 and the hyperbola is the line of zero discriminant

Figure 4.2: Region (I) is forbidden as $F(S) < 0$ on $[-1, 1]$

- Region II: In this region $\varepsilon < 0$. The leading coefficient in $F(S)$ is positive, hence the parabola is opening upwards. Also, $F(-1) > 0$ and $F(1) < 0$. One of the roots lies inside the interval $[-1, 1]$ and one root greater than 1 lies outside the interval which is shown in Figure 4.3.

Figure 4.3: Region (II)- The part $[-1, S_1]$ of the interval $[-1, 1]$ is admissible.

- Region III: In this region $\varepsilon < 0$. The leading coefficient in $F(S)$ is positive, hence the parabola is opening upwards. Also, $F(-1) > 0$ and $F(1) > 0$. Both the roots lie inside the interval $[-1, 1]$ which is shown in Figure 4.4.

Figure 4.4: Region (III)- The parts $[-1, S_1]$ and $[S_2, 1]$ are admissible.

- Region IV: In this region $\varepsilon < 0$. The leading coefficient in $F(S)$ is positive, hence the parabola is opening upwards. Also, $F(-1) > 0$ and $F(1) > 0$. There are no roots since the determinant is less than 0 which is shown in Figure 4.5.

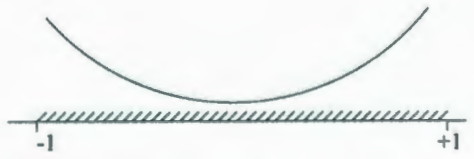

Figure 4.5: Region (IV)- The whole interval $[-1, 1]$ for S is admissible.

- Region V: In this region $\varepsilon < 0$. The leading coefficient in $F(S)$ is positive, hence the parabola is opening upwards. Also, $F(-1) > 0$ and $F(1) > 0$. Both the roots are large and positive which is shown in Figure 4.6.

Figure 4.6: Region (V)- The whole interval $[-1, 1]$ for S is admissible.

- Region VI: In this region $\varepsilon > 0$. The leading coefficient in $F(S)$ is negative, hence the parabola is opening downwards. Also, $F(-1) < 0$ and $F(1) < 0$. Both the roots are large and negative which is shown in Figure 4.7.

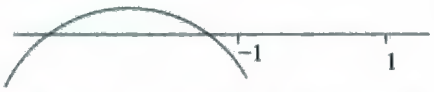

Figure 4.7: Region (VI) is forbidden as $F(S) < 0$ on $[-1, 1]$.

- Region VII: In this region $\varepsilon > 0$. The leading coefficient in $F(S)$ is negative, hence the parabola is opening downwards. Also, $F(-1) > 0$ and $F(1) < 0$. One of the roots lies inside the interval $[-1, 1]$ and the other root is less than -1 which is shown in Figure 4.8.

Figure 4.8: Region (VII)- The part $[-1, S_2]$ of the interval $[-1, 1]$ is admissible.

- Region VIII: In this region $\varepsilon > 0$. The leading coefficient in $F(S)$ is negative, hence the parabola is opening downwards. Also, $F(-1) < 0$ and $F(1) < 0$. There are no roots, since the determinant is less than 0 which is shown in Figure 4.9.

Figure 4.9: Region (VIII) is forbidden for S.

- Region IX: In this region $\varepsilon > 0$. The leading coefficient in $F(S)$ is negative, hence the parabola is opening downwards. Also, $F(-1) < 0$ and $F(1) < 0$. Both the roots lie inside the interval $[-1, 1]$ which is sown in Figure 4.10.

Figure 4.10: Region (IX)- The part $[S_1, S_2]$ of the interval $[-1, 1]$ is admissible.

- Region X: In this region $\varepsilon > 0$. The leading coefficient in $F(S)$ is negative, hence the parabola is opening downwards. Also, $F(-1) > 0$ and $F(1) > 0$. Both the roots lie outside the interval $[-1, 1]$, with one root lesser than -1 and the second root greater than 1 which is shown in Figure 4.11.

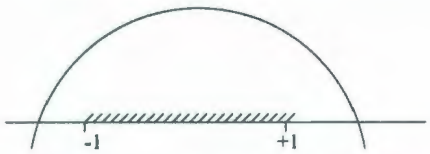

Figure 4.11: Region (X)- The whole interval $[-1, 1]$ for S is admissible.

4.2 Analysis of the polynomial $G(\rho)$

The separating lines for the equation $G(\rho) = \varepsilon\rho^2 + 2\rho + A = 0$ separate regions with different number of roots on the "good" interval $[1, \infty)$.

These lines are:

1. The A-axis ($\varepsilon = 0$);

2. The discriminant $D = 0$:

$$\varepsilon = \frac{1}{A}; \tag{4.6}$$

3. One root is $+1$:

$$\varepsilon + 2 + A = 0. \tag{4.7}$$

Figure 4.12 presents the plot of the separating lines.

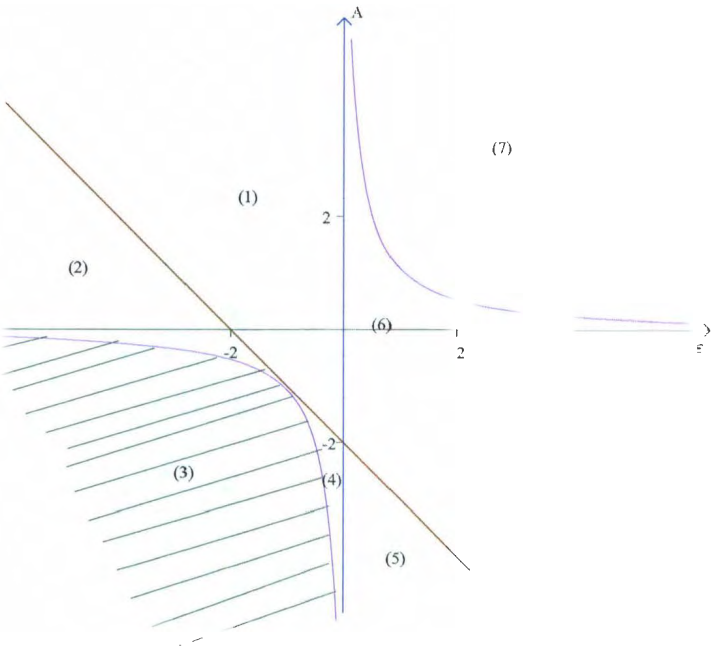

Figure 4.12: Separating lines for $G(\rho)$. The straight line is $F(1) = 0$ and the hyperbola is the set $D = 0$

In Figure 4.12, the hyperbola corresponds to the separating line (4.6); the line passing through the third quadrant corresponds to the separating line (4.7). From Figure 4.12 we notice that the separating lines divide the parametric space A-ε into seven different regions denoted by numbers from (1) to (7). The graphs below show

schematically the position of the real roots of $G(\rho)$ relative to the interval $[1, \infty)$ in the cases corresponding to different regions as shown in Figure 4.12.

- Region 1: In this region $\varepsilon < 0$. The leading coefficient in $G(\rho)$ is negative, hence the parabola is opening downwards. One of the roots lies inside the interval $[1, \infty)$ and the other root lies outside the interval i.e. it is less than 1 which is shown in Figure 4.13.

Figure 4.13: Region (1)- The part $[1, \rho_2]$ of $[1, \infty)$ is admissible.

- Region 2: In this region $\varepsilon < 0$. The leading coefficient in $G(\rho)$ is negative, hence the parabola is opening downwards. Both roots lie outside the interval $[1, \infty)$ as shown in Figure 4.14.

Figure 4.14: Region (2) is forbidden as $G(\rho) < 0$ on $[1, \infty)$.

- Region 3: In this region $\varepsilon < 0$. The leading coefficient in $G(\rho)$ is negative, hence the parabola is opening downwards. There are no roots since the discriminant is less than zero as shown in Figure 4.15.

Figure 4.15: Region (3) is forbidden.

- Region 4: In this region $\varepsilon < 0$. The leading coefficient in $G(\rho)$ is negative, hence the parabola is opening downwards. Both roots lie inside the interval $[1, \infty)$ as shown in Figure 4.16.

Figure 4.16: Region (4)- The part $[\rho_1, \rho_2]$ of the interval $[1, \infty)$ is admissible.

- Region 5: In this region $\varepsilon > 0$. The leading coefficient in $G(\rho)$ is positive, hence the parabola is opening upwards. One of the roots lies inside the interval $[1, \infty)$ and the other root lies outside the interval, i.e. it is less than 1 as shown in Figure 4.17.

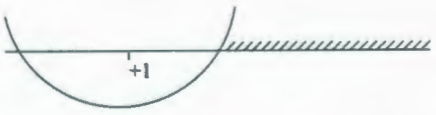

Figure 4.17: Region (5)- The part $[\rho_2, \infty)$ of the interval $[1, \infty)$ is admissible.

- Region 6: In this region $\varepsilon > 0$. The leading coefficient in $G(\rho)$ is positive, hence the parabola is opening upwards. Both roots lie outside the interval $[1, \infty)$ as shown in Figure 4.18.

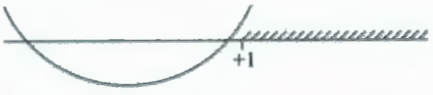

Figure 4.18: Region (6)- The whole interval $[1, \infty)$ is admissible.

- Region 7: In this region $\varepsilon > 0$. The leading coefficient in $G(\rho)$ is positive, hence the parabola is opening upwards. There are no real roots in this region which

is shown in Figure 4.19.

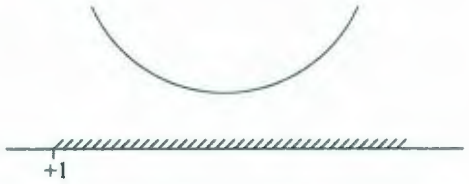

Figure 4.19: Region (7)- The whole interval $[1, \infty)$ is admissible.

4.3 Combined analysis. Types of trajectories

In this section we describe various bounded cases of motion and classify different types of trajectories.

The particle P is orbiting over a two-dimensional surface in the phase space, which is the intersection of a three-dimensional energy surface and a three-dimensional level surface of the integral H_1 (or H_2) in the four-dimensional phase space.
The physically observable orbit of the particle lies in the configuration space, which is the (x, y)-plane. The physical orbit in the two-dimensional (x, y) plane is the projection of the mathematical trajectory in the phase space (x, y, p_x, p_y) obtained by simply ignoring the values of p_x and p_y. In order to characterize the qualitative bahaviour of physical orbits in different cases, we will describe the boundaries of the domains in the (x, y) plane swept out by them. These boundaries are level curves of R and σ corresponding to roots of the polynomials $F(S)$ and $G(\rho)$.

We combine Figures 4.1 and 4.12 to know more precisely the boundaries of the particle's orbit for the values (A, ε) in different regions of the combined plot. Some types of trajectories are as follows.

(P1) A trajectory of the particle may lie within an elliptic annulus encircling the two fixed masses.

(P2) A trajectory may be bounded by an ellipse and an hyperbola with foci at the two fixed masses.

(P3) A trajectory may be confined within a single ellipse encircling the two fixed masses and come arbitrarily close to the masses.

The P-classification is found in Strand and Reinhardt [17]. In some regions of the combined plot, the dynamics of the system will not be possible, as we will explain in this section.

In the combined plot of Figures 4.1 and 4.12 with $\beta = 0.1$ some of the regions cannot be easily seen and analyzed due to uneven scaling. Hence for better understanding of the regions we are presenting the plots for $\beta = 0.375$. (Yet the value of $\beta = 0.1$ is used in computations throughout).
Figure 4.20 is the combined plot of the Figures 4.1 and 4.12. The following are the observations from the plot on Figure 4.20.

In the regions (I), (VI), (VIII) the value of $F(S)$ is negative on $[-1, 1]$. However, in the equation (3.32) for the denominator to be positive $F(S)$ must be > 0 on $[-1, 1]$ or on its part. Therefore, the dynamics of the system is not possible and so the regions (I), (VI), (VIII) in the parametric space are forbidden. Similarly, in the regions (2), (3) the value of $G(\rho)$ is negative on $[1, \infty)$. However, in the equation (3.31) for the denominator to be positive, $G(\rho)$ must be > 0 on $[1, \infty)$ or on a part of it. Therefore, the dynamics of the system is not possible and so the regions (2), (3) in the parametric space are forbidden. Also, region (7) is a subset of the forbidden region (VIII), hence region (7) is always forbidden, despite the fact that $G(\rho) > 0$ in it.

In the regions (IV), (V), (X) the value of $F(S)$ is positive on $[-1, 1]$ and hence all the three regions can be identified the same for the purpose of classification of real roots of $F(S)$ relative to $[-1, 1]$. In the regions (6) and (7) the value of $G(\rho)$ is positive on $[1, \infty)$ and hence the two regions can be identified the same for the purpose of classification of real roots of $G(\rho)$ relative to $[1, \infty)$. But region (7) is forbidden as we have shown. From the above observations, the number of regions for the equation (3.31) gets reduced to four and for the equation (3.32) the number of regions gets also reduced to four. We identify the regions as (A),..,(D) for the polynomial $F(S)$ and (a),..,(d) for the polynomial $G(\rho)$. The reduced plot is shown in Figure 4.21.

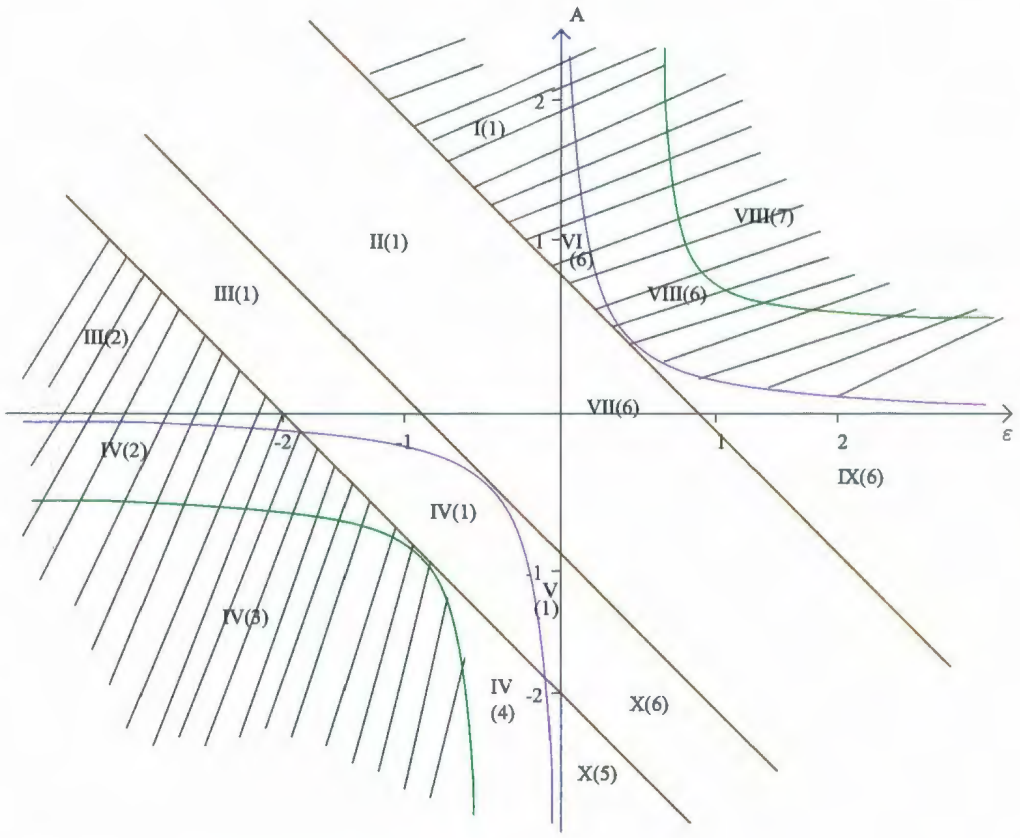

Figure 4.20: A combined plot of Figures 4.1 and 4.12

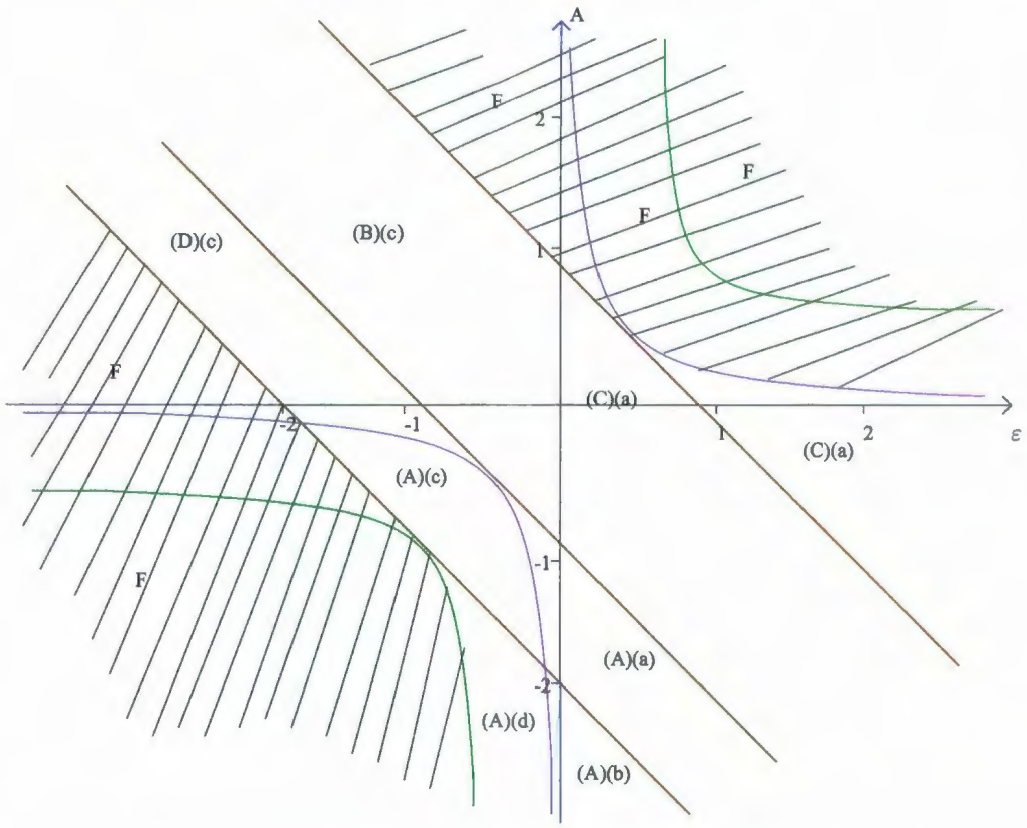

Figure 4.21: A reduced combined plot of Figures 4.1 and 4.12 with forbidden regions

The forbidden region in Figure 4.21 is denoted by (F).

According to the position of roots of the polynomial $F(S)$ defined by (4.2) relative to the interval $[-1, 1]$, the regions on Figure 4.21 are characterized as follows.

- Region (A): $F(S) > 0$ on $[-1, 1]$ (corresponds to regions IV, V and X);
- Region (B): $F(S) > 0$ on $[-1, S_1)$ (corresponds to region II);
- Region (C): $F(S) > 0$ on (S_1, S_2) (corresponds to region VII);
- Region (D): $F(S) > 0$ on $[-1, S_1)$ and $[S_2, 1)$ (corresponds to region III).

Here S_1 and S_2 are the roots of the equation $F(S) = 0$ in $[-1, 1]$ (if one or two of them exist).

According to the position of roots of the polynomial $G(\rho)$ defined by (4.1) relative to the interval $[1, \infty)$ the regions on Figure 4.21 are characterized as follows.

- Region (a): $G(\rho) > 0$ on $[1, \infty)$ (corresponds to region 6);
- Region (b): $G(\rho) > 0$ on $[\rho_1, \infty)$ (corresponds to region 5);
- Region (c): $G(\rho) > 0$ on $[1, \rho_1]$ (corresponds to region 1);
- Region (d): $G(\rho) > 0$ on $[\rho_1, \rho_2]$ (corresponds to region 4).

Where ρ_1 and ρ_2 are the possible roots of the equation (4.1) in $[1, \infty)$.

We investigate the motion of the particle by analyzing different combinations of the regions (A)—(D) with regions (a)—(d) in Figure 4.21. This is not an exhaustive list of all possible combinations of regions. We consider bounded cases of motion everywhere except in the end of this section and in Section 5.1. In all the graphs below the shaded region is where the particle orbits.

1. Let us consider the combination of regions (A) and (c). The only boundary is given by the equation $R = \rho_1$, according to Section 4.3, so the motion of the particle is bounded by an ellipse is displayed in Figure 4.22.

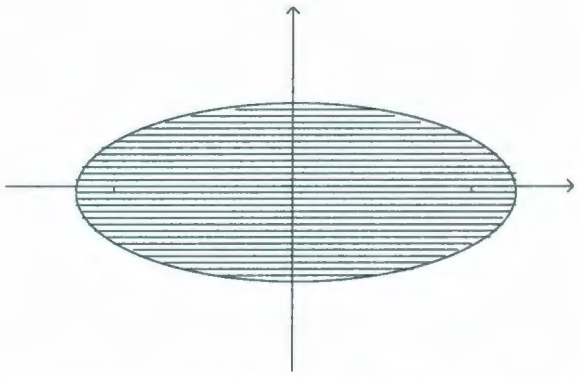

Figure 4.22: The orbit of type (Ac) is bounded by an ellipse

2. Let us consider the combination of regions (A) and (d). The bounds of motion are given by the inequality $\rho_1 \leq R \leq \rho_2$, according to Section 4.3, so the motion of the particle is confined within an elliptic annulus encircling the two fixed masses is displayed in Figure 4.23.

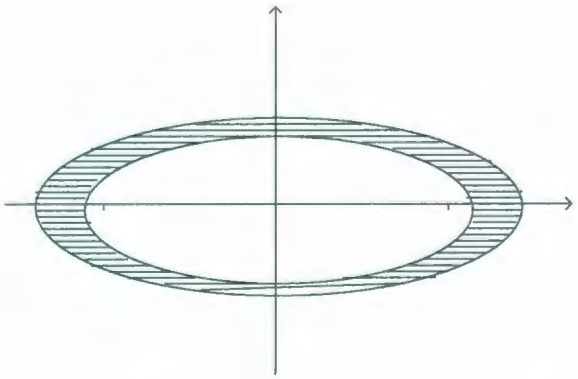

Figure 4.23: The orbit of type (Ad) is confined within an elliptic annulus

3. Let us consider the combination of regions (B) and (c). The boundary is given by the equations $S \leq S_1$ for hyperbola and $R = \rho_1$ for ellipse according to Section 4.3, so the motion of the particle is confined between an ellipse and an hyperbola is displayed in Figure 4.24.

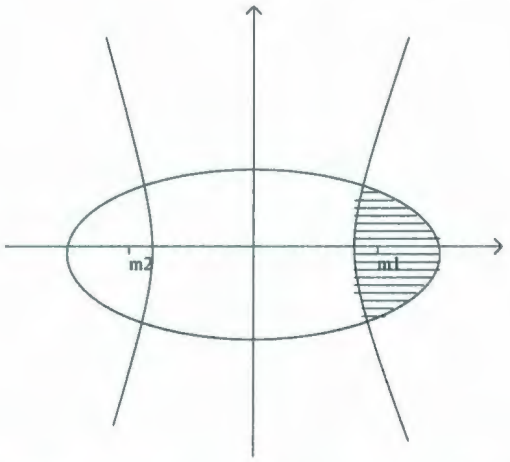

Figure 4.24: The orbit of type (Bc) is confined within an ellipse and a hyperbola

Figures 4.22, 4.23 and 4.24 correspond to Figures 7, 8 and 9 of Strand and Reinhardt [17].

Some combinations of regions, say, (Bd), (Cc), (Cd) have no place on the diagram Figure 4.21. The corresponding combinations of intervals for ρ and S, though mathematically conceivable, turn out to be dynamically impossible. In addition to the above analysis, this can be demonstrated by simple physical arguments as we will show now.

4. Let us consider the combination of regions (B), (d). The boundaries are given by inequality $\rho_1 \leq R \leq \rho_2$ for the ellipse and $S \leq S_1$ for the hyperbola, from Section 4.3, so the motion of the particle would be confined between two ellipses and has an hyperbola as an additional boundary is shown in Figure 4.25. Suppose the particle P makes a turning point above the x-axis at the hyperbola, then it must come to a complete stop and the acceleration vector should have a positive y component which is clearly impossible (since the masses are situated below).

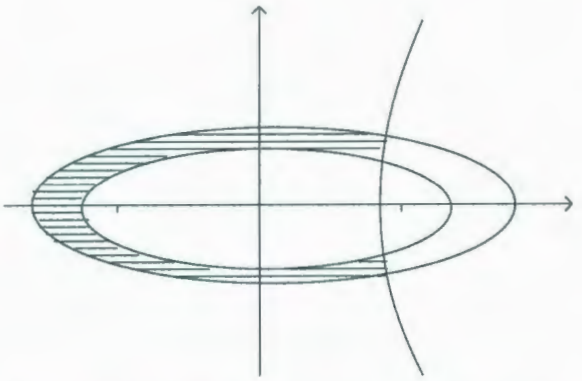

Figure 4.25: Impossible orbit is bounded by two ellipses and a hyperbola

5. Let us consider the combination of regions (C) and (c). The boundary is given by the equations $R = \rho_1$ for ellipse and $S_1 \leq S \leq S_2$ for hyperbola according to Section 4.3, so the motion of the particle would be confined to the region bounded by the ellipse and the hyperbola. Suppose the particle P makes a turn at the hyperbola near to the left mass. The force of the right mass is thus prevailing on the particle. When the particle approaches the neighborhood of the right mass, it is therefore impossible for it to turn around the right fixed mass, which is displayed in Figure 4.26.

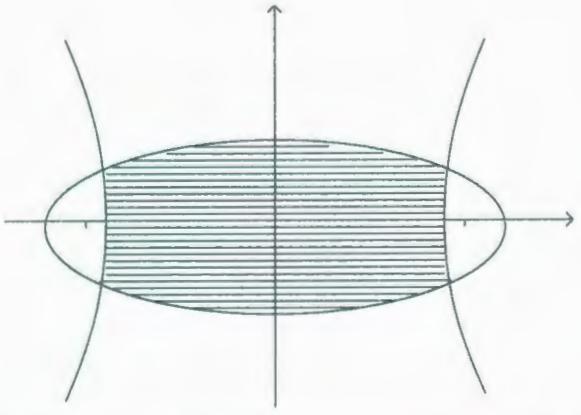

Figure 4.26: Impossible orbit is confined to a region bounded by an ellipse and an hyperbola

6. Let us consider the combination of regions (C) and (d). The boundary is given by the inequalities $\rho_1 \leq R \leq \rho_2$ for ellipses and $S_1 \leq S \leq S_2$ for the hyperbolas according to Section 4.3, so the motion of the particle would be confined to the region bounded by two ellipses and two branches of hyperbola. This case is impossible because the two masses are situated below the orbit.

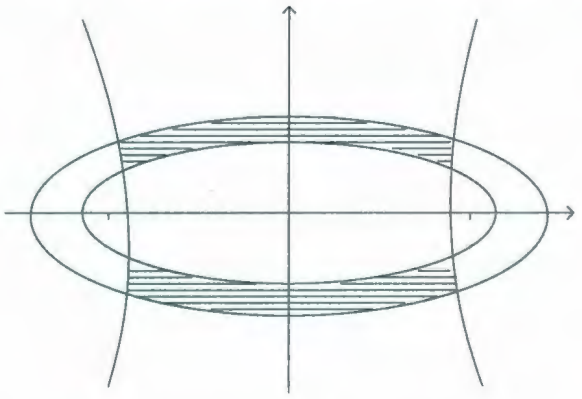

Figure 4.27: Impossible orbit is confined to a region bounded by two ellipses and two branches of a hyperbola

4.4 Dependence on time

In this section we describe the correspondence between the physical time t and the artificial time τ, and discuss how periodic motions in τ lead to both bounded and unbounded cases of motions in physical space-time.

The original Hamiltonian system H with two degrees of freedom is written with respect to time t. One integral of motion for the Hamiltonian system is the Hamiltonian itself. The motion occurs along trajectories on the energy surfaces $H = E$. If Liouville's theorem in Section 3.1 is applicable, then there is a change in the time factor. The new time that is associated with each of the auxiliary Hamiltonian systems is τ. The trajectories determined by the combination of the auxiliary Hamiltonian systems are the same as those of the original Hamiltonian system. However the new time variable τ that is associated with the independent Hamiltonian systems is

not identical to the time variable t that is associated with the original Hamiltonian system; specifically $t(\tau)$ is defined by (3.16).

We have the equations (3.31) and (3.32). Consider, say, the case (A) where $F(S) > 0$ on $[-1, 1]$. Then the integral

$$\tau_S = \frac{1}{2}\int_{-1}^{1} \frac{dS}{\sqrt{(1-S^2)F(S)}}, \tag{4.8}$$

converges and the equation (3.32) defines a periodic function $F(S)$ with period $2\tau_S$. A sample graph of $S(\tau)$ is presented in Figure 4.28.

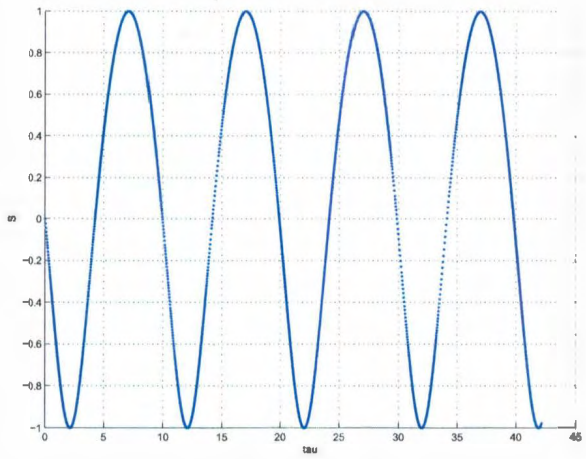

Figure 4.28: Graph of $S(\tau)$ with values $(A, \varepsilon) = (-0.387, -0.0901)$

If $F(S)$ has one or two roots on $[-1, 1]$, then the interval of integration $[-1, 1]$ in the formula for τ_S in (4.8) should be replaced by one of the intervals $[-1, S_1]$, $[S_1, S_2]$ or $[S_2, 1]$ (on which $F(S) > 0$).

If $G(\rho)$ has one root on $[1, \infty)$ and $\varepsilon < 0$, so that $G(\rho) > 0$ on $[1, \rho_2)$, then the function $\rho(\tau)$ defined by (3.31) is periodic with period $2\tau_\rho$, where

$$\tau_\rho = \frac{1}{2}\int_{1}^{\rho_2} \frac{d\rho}{\sqrt{(\rho^2-1)G(\rho)}}. \tag{4.9}$$

If $G(\rho)$ has two roots ρ_1, ρ_2 on $[1, \infty)$, then $\rho(\tau)$ has period $2\tau_\rho$, with

$$\tau_\rho = \frac{1}{2}\int_{\rho_1}^{\rho_2} \frac{d\rho}{\sqrt{(\rho^2-1)G(\rho)}}. \tag{4.10}$$

Let us now mention the unbounded cases of motion.

Let us consider the polynomial $G(\rho)$ in the case (6), where $\varepsilon > 0$.

As $\rho \to \infty$ we have

$$G(\rho) \approx \varepsilon\rho^2 + O(\rho) > 0.$$

Hence

$$(\rho^2-1)G(\rho) \approx \varepsilon\rho^4.$$

Substituting in the equation (3.32) we obtain

$$\frac{d\rho}{\rho^2\sqrt{\varepsilon}} \approx \pm 2\, d\tau.$$

Integrating, we get

$$2(\tau - \tau_*) \approx \mp\frac{1}{\rho\sqrt{\varepsilon}},$$

or

$$\rho \approx \mp\frac{1}{2\sqrt{\varepsilon}(\tau-\tau_*)}. \tag{4.11}$$

As $\tau \to \tau_*^-$, then $\rho \to +\infty$.

At a certain time $\tau = \tau_*$, the particle moves out from the system and goes to infinity. This happens because the integral

$$\tau(\infty) = \frac{1}{2}\int^{\infty} \frac{d\rho}{\sqrt{(\rho^2-1)G(\rho)}}.$$

converges. A sample graph of $\rho(\tau)$ in the case of unbounded motion is presented in Figure 4.29.

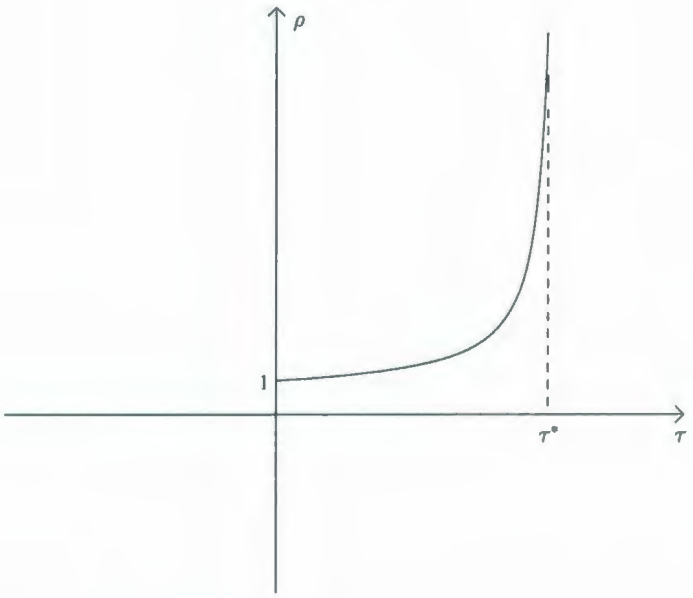

Figure 4.29: Sample graph of $\rho(\tau)$ in the case of unbounded motion

Chapter 5

Applications and numerical results

5.1 Escape velocities

We first discuss the escape velocity for the Keplerian (two body) problem, which we understand here as a problem of a particle with negligible mass orbiting around a massive fixed center. Depending on initial conditions, the orbit of the particle can be elliptical (in particular, circular), parabolic or hyperbolic. A particle following an elliptic orbit stays within a fixed distance from the central mass forever. Given location of the particle and direction of the velocity vector, small magnitude of the velocity corresponds to elliptic motion, while large magnitude corresponds to hyperbolic motion. The borderline value of the magnitude of the velocity vector corresponds to a parabolic motion and it is called the escape velocity. Thus, the escape velocity is the minimum velocity that the particle should attain in order to leave a neighbourhood of the massive center.

In a similar way, we define the first escape velocity for our model. Suppose that during an initial time period the planet is close to m_1, so the force of attraction to m_1 is much greater than the force of attraction to m_2. Neglecting the influence of m_2 makes the system similar to that of the Keplerian problem. However the influence of m_2 cannot be neglected over a long time interval. Every coil of the orbit around m_1 is only approximately an ellipse. The directions and lengths of the major and minor

axes gradually change and there are two possible scenarios:

1. The planet still remains locked in a bounded region containing m_1, but not m_2, as shown in Figure 4.24.

2. The influence of m_2 may become strong enough to destroy the elliptical pattern of orbiting around m_1 and to qualitatively change the local character of the motion. In this case, the global orbit will either be unbounded or it will fill a region containing both m_1 and m_2 as shown in Figure 4.22.

The minimum velocity (at a given initial point, in given direction) required for scenario 2 to happen will be called the first escape velocity. We denote it by v_b.

We define the second escape velocity of the particle as the minimum velocity that the particle should attain so that it escapes from the whole system i.e. from the gravitational influence of the two fixed masses. We denote the second escape velocity by v_s. (The subscripts "b" and 's" correspond to "body" and "system")

If the particle escapes from the entire system then it must necessarily escape from the influence of m_1. In terms of escape velocities it just shows that $v_b \leq v_s$.

Let the particle P be initially placed between the two fixed masses. Let α be the angle with which the particle starts from its initial position as shown in Figure 5.1.

As before we assume $m_1 + m_2 = 1$, $m_2 - m_1 = \beta$ and $b = 1$.

We derive explicit formulas to calculate the two escape velocities v_b and v_s.

At time $t = 0$, the position of the particle is $(x_0, 0)$, where $-1 < x_0 < 1$. The assumption $y_0 = 0$ implies that $R = 1$ and hence $\rho = 1$.

Also we have a relation $x = R\cos\sigma = RS$, whence the initial values of S is x_0.

Therefore the initial values are

$$S = x_0; \quad \rho = 1.$$

Let us begin by deriving the second escape velocity, which is simpler.

The energy is calculated as

$$E = \frac{v_0^2}{2} - \frac{m_1}{1 - x_0} - \frac{m_2}{1 + x_0}. \tag{5.1}$$

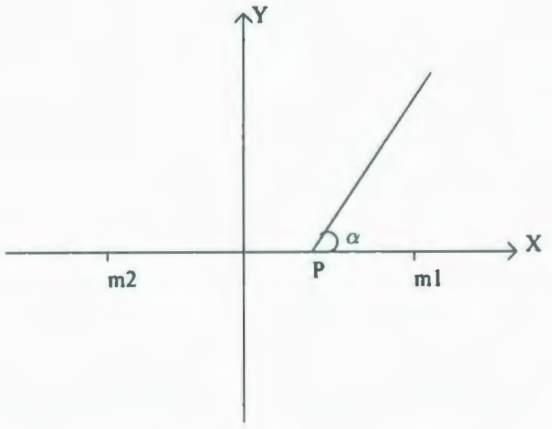

Figure 5.1: Initial position of the particle P between the two masses, which are fixed at $(-1,0)$, $(1,0)$, in the escape velocity problem

Orbits are bounded if and only if $E < 0$, or equivalently

$$v_0^2 < 2\left(\frac{m_1}{1-x_0} - \frac{m_2}{1+x_0}\right) = 2\left(\frac{1-\beta x_0}{1-x_0^2}\right), \tag{5.2}$$

which yields the second escape velocity

$$v_s = \sqrt{2\left(\frac{1-\beta x_0}{1-x_0^2}\right)}. \tag{5.3}$$

The condition $v_0 > v_s$ is not only necessary but also sufficient for the particle to escape to ∞. Indeed, the analysis for $G(\rho)$ in Section 4.2 shows that the case when $\varepsilon > 0$ and both the roots ρ_1, ρ_2 are greater than 1 does not occur. For $\epsilon > 0$ the particle cannot be confined in an elliptic region $\rho \leq \rho_1$.

We now derive the first escape velocity v_b.

The particle does not escape the influence of the mass m_1 if it is confined to the unshaded region within the ellipse to the right from the hyperbola on Figure (4.11). Existence or non-existence of such region is controlled by or depends on the boundary in the parametric space corresponding to one of the roots of $F(S)$ being $+1$ and the corresponding separating line (4.5) passes across the third quadrant on Figure 4.1.

The second integral A (3.5) is calculated according to (3.3):

$$A = p_R^2(R^2 - b^2) - R(m_1 + m_2) - 2ER^2. \tag{5.4}$$

Despite the factor $R^2 - b^2 = 0$ at $t = 0$, we cannot claim that the term $p_R^2(R^2 - b^2)$ in (5.4) vanishes, because $p_R \longrightarrow \infty$ as $R \longrightarrow b$ according to (2.17). Instead we have, by (2.15)

$$p_R^2(R^2 - b^2) = (p_x \cos\sigma\sqrt{R^2 - b^2} + p_y R \sin\sigma)^2.$$

At $t = 0$, $\cos\sigma = x_0$ and $p_y = v_0 \sin\alpha$. Hence

$$\begin{aligned} p_R^2(R^2 - b^2) &= p_y^2 R^2 \sin^2\sigma \\ &= 1(1 - \cos^2\sigma)v^2 \sin^2\alpha \\ &= (1 - x_0)^2 v^2 \sin^2\alpha. \end{aligned}$$

Substituting this in (5.4) we get

$$A = (1 - x_0)^2 v^2 \sin^2\alpha - 1 - 2E. \tag{5.5}$$

From (4.5) and (5.5) we obtain

$$v_b = \sqrt{\frac{1 - 2\beta}{(1 - x_0^2)\sin^2\alpha}}. \tag{5.6}$$

The minimum first escape velocity, corresponding to $\sin\alpha = \frac{\pi}{2}$, i.e. to the vertical direction of the initial velocity vector, is

$$v_{bmin} = \sqrt{\frac{1 - 2\beta}{(1 - x_0^2)}}. \tag{5.7}$$

(If $\beta > 0.5$, i.e. $m_2 > 0.75$ and $m_1 < 0.25$, then there is no minimum first escape velocity and the particle cannot be confined close to the mass m_1).

Table 5.1 displays the minimum first escape velocity v_{bmin} and the second escape velocity v_s for the particle P placed at different positions between the two fixed masses.

Table 5.1: Different values of the minimum first escape velocity and the second escape velocity

Position of the particle	First escape velocity	Second escape velocity
0.10	0.898	1.348
0.25	0.923	1.385
0.50	1.032	1.549
0.65	1.176	1.765
0.85	1.697	2.546

5.2 Collision of the planet with a star

In this section we discuss an interesting application of the theory which we had dealt with in the previous chapters.

As before, we assume $m_1 + m_2 = 1$, $m_2 - m_1 = \beta$, $b = 1$.

We are interested to investigate the initial velocity of the particle P and also the angle at which the particle P should start from its initial position so that it hits (or collides with) one of the fixed masses.

The collision of the particle with one of the fixed masses may occur on an immediate approach or after N revolutions where $N = 0, 1, 2, ...$(Here $N = 0$ corresponds to an immediate approach).

Let the initial position of the particle P be $(x_0, y_0) = (0, 1)$.

The initial distances from the particle P to the two fixed masses are

$$r_1 = r_2 = \sqrt{1 + y_0^2} = \sqrt{2}. \tag{5.8}$$

We derive the formulas for the initial velocity v_0 and the angle ψ.

The initial values of elliptic coordinates are found by subtracting the equations (2.6) and we get $\cos\sigma_0 = S_0 = 0$. Therefore $\sigma_0 = \pm\frac{\pi}{2}$. We choose positive sign because $y_0 > 0$.

Adding the equations (2.6) we get $R_0 = \rho_0 = r_1 = r_2 = \sqrt{2}$.

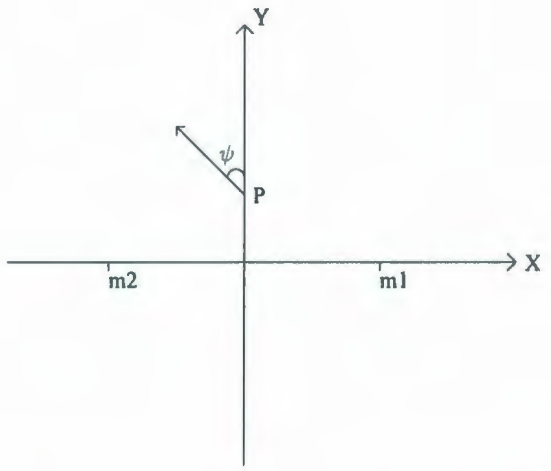

Figure 5.2: Two masses m_1 and m_2 placed at $x = 1$ and $x = -1$ respectively and the particle P is placed at $y = 1$

According to the assumption $2E = \varepsilon$, (5.8) and the formula (2.11) for energy, we have

$$\begin{aligned} E &= \frac{v^2}{2} - \frac{m_1}{r_1} - \frac{m_2}{r_2} \\ &= \frac{v^2}{2} - \frac{1}{\sqrt{2}}. \end{aligned}$$

Therefore the initial velocity of the particle P is

$$v_0 = \sqrt{\varepsilon + \sqrt{2}}. \tag{5.9}$$

The second integral A (3.5) is calculated according to (3.3):

$$A = p_R^2(R^2 - b^2) - R(m_1 + m_2) - 2ER^2. \tag{5.10}$$

So, at $t = 0$, we have $p_y = v_0 \cos\psi$ by (2.6), where (p_x, p_y) is the initial momentum of the particle. From (2.17) we have

$$\begin{aligned} p_R^2(R^2 - b^2) &= (p_x \cos\sigma\sqrt{R^2 - b^2} + p_y R \sin\sigma)^2 \\ &= R^2 p_y^2 \sin^2\sigma \end{aligned}$$

$$= 2(1-\cos^2\sigma)v_0^2\cos^2\psi$$
$$= 2v_0^2\cos^2\psi.$$

Substituting in (5.10) we get

$$A = 2v_0^2\cos^2\psi - \sqrt{2}(m_1+m_2) - 2E(\sqrt{2})^2$$
$$= 2v_0^2\cos^2\psi - 2 - 2\varepsilon.$$

Therefore the relation between the initial velocity v_0 and the values A and ε of the integrals of motion is

$$\psi = \arccos\sqrt{\frac{A+2+2\varepsilon}{2v_0^2}}. \tag{5.11}$$

We know v_0 from (5.9), so given A, ε we can evaluate the angle ψ. Now we need to find A and ε to ensure that the particle P collides with one of the fixed masses.

The final values corresponding to the level lines when the particle hits the right fixed mass are

$$\begin{aligned} S &= 1, \\ \rho &= 1. \end{aligned} \tag{5.12}$$

The final values corresponding to the level lines when the particle hits the left fixed mass are

$$\begin{aligned} S &= -1, \\ \rho &= 1. \end{aligned} \tag{5.13}$$

The level curve of ρ is an interval which is a limiting case of an ellipse and the level curve of σ is an hyperbola whose asymptotes tend to ∞ along the x-axis as discussed in Section 4.3.

A schematic diagram of the level curves corresponding to the final values is shown in Figure 5.3.

Denote the artificial time τ when the particle collides with a fixed mass by τ_*. (The physical time t will be different, in accordance with (3.16).)

Figure 5.4 is a sample graph of the periodic function $\rho(\tau)$ since the motion begins until the particle hits the right fixed mass. The first interval of growth is an incomplete half period. A corresponding analysis has been carried out in Section 4.5.

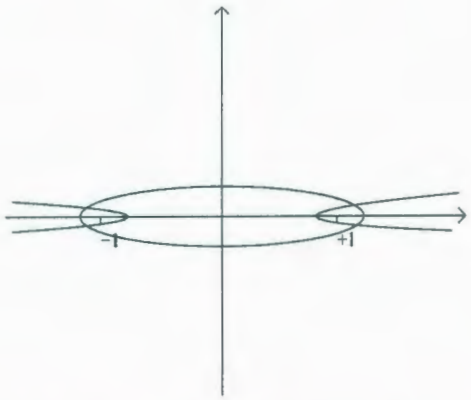

Figure 5.3: Level curves of R and σ corresponding to the particle approaching one of the fixed masses

When the particle hits the right fixed mass, the total time elapsed since the motion started is given by

$$\begin{aligned} \tau_{total1} &= \tau_\rho N_\rho + \phi_\rho \tau_\rho \\ &= (N_\rho + \phi_\rho)\tau_\rho, \end{aligned} \tag{5.14}$$

where

N_ρ - number of full half periods of $\rho(\tau)$ before the particle hits the right fixed mass;

τ_ρ - half period of the function $\rho(\tau)$;

ϕ_ρ - initial incomplete fraction of the half period $(0 < \phi_\rho < 1)$.

During the initial segment of the trajectory the value of ρ increases from $\rho_0 = \sqrt{2}$ to the maximum value $\rho_{max} = \rho_2$, which is the bigger root of $G(\rho)$, and the equation $\rho = \rho_2$ determines the ellipse enclosing the whole trajectory. Then ρ goes down from ρ_{max} to $\rho_{min} = 1$. The minimum occurs when the trajectory crosses the horizontal axis between the two masses (in the right neighborhood of the left fixed mass). Then ρ increases again until it reaches the maximum for the second time (the right loop of the trajectory). Then ρ goes down to 1, which is attained at the moment of the

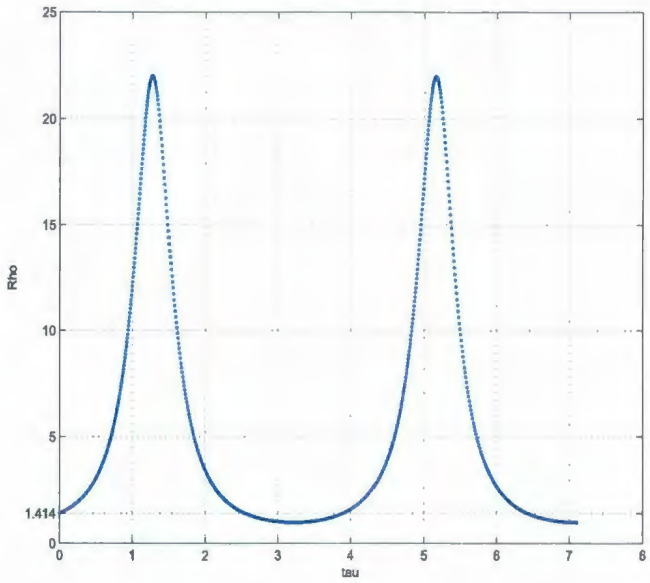

Figure 5.4: Plot of $\rho(\tau)$ showing 1 incomplete and 3 complete half periods

collision. Therefore, τ_{total1} = an initial incomplete half-period+ three full half periods. Hence $\tau_{total1} = (\phi_\rho + 3)\tau_\rho$.

Similarly, Figure 5.5 is a sample graph of the periodic function $S(\tau)$ until the particle hits the right fixed mass.

When the particle hits the right fixed mass, the total time elapsed since the motion started is given as

$$\begin{aligned} \tau_{total2} &= \tau_S N_S + \phi_S \tau_S \\ &= (N_S + \phi_S)\tau_S, \end{aligned} \tag{5.15}$$

where

N_S - number of full half periods of $S(\tau)$ before the particle hits the right star;

τ_S - half period of the function $F(S)$;

ϕ_S - initial incomplete fraction of half period $(0 < \phi_S < 1)$.

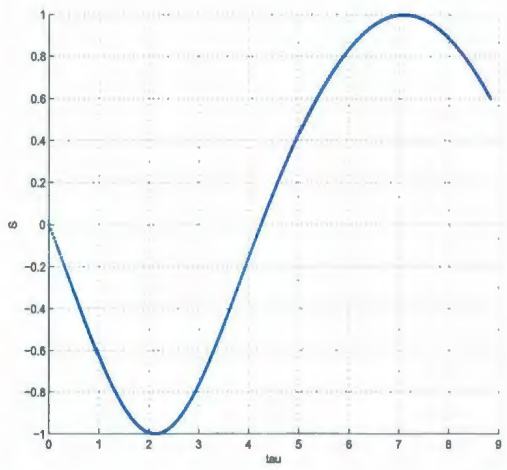

Figure 5.5: Plot of $S(\tau)$ showing an incomplete half period and 1 full half period

The quantities ϕ_ρ, ϕ_S will be referred to as phase shifts.

The initial value of S is 0. Then S goes down until it reaches the value -1 and this happens when the trajectory intersects the horizontal axis on the left from the left fixed mass. Then S goes up, passes the value 0 when the trajectory intersects the y-axis, and finally reaches the value $+1$ when it hits the right fixed mass. Therefore, τ_{total2}=an incomplete half-period+one full half period. Hence τ_{total2}=$(\phi_S + 1)$ half-periods.

Since

$$\tau_{total1} = \tau_{total2}, \tag{5.16}$$

(the total time elapsed till the collision), combining equations (5.14) and (5.15) we get

$$\frac{\phi_\rho + N_\rho}{\phi_S + N_S} = \frac{\tau_S}{\tau_\rho}. \tag{5.17}$$

The half periods τ_S and τ_ρ are represented by complete elliptic integrals (4.8) and (4.9), which depend on A and ε.

We are considering the case of bounded motion, i.e. $\varepsilon < 0$. Let us write (4.9) in

the form

$$\frac{1}{2}\left(\frac{1}{\sqrt{-\varepsilon}}\int_1^{\rho_2}\frac{d\rho}{\sqrt{(\rho^2-1)(\rho-\rho_1)(\rho_2-\rho))}}\right), \tag{5.18}$$

where $\rho_1 < -1$ and $\rho_2 > 1$ are the roots of the polynomial $G(\rho)$ given by:

$$\rho_1 = \frac{-1-\sqrt{4-4A\varepsilon}}{2\varepsilon}, \quad \rho_2 = \frac{-1+\sqrt{4-4A\varepsilon}}{2\varepsilon}.$$

Evaluating (5.18) in Maple software, we obtain

$$\tau_\rho = \frac{2K\left(\sqrt{\frac{(\rho_2-1)(-\rho_1-1)}{(\rho_2+1)(1-\rho_1)}}\right)}{\sqrt{-\varepsilon}\sqrt{\rho_2-\rho_2\rho_1+1-\rho_1}}, \tag{5.19}$$

where K is the complete elliptic integral of first kind, which in Maple is known as `EllipticK`.

We have the following scheme, showing the position of the roots ρ_1 and ρ_2, which corresponds to the region (1) in Figure 4.2.

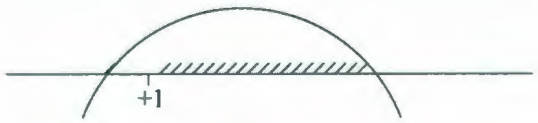

Figure 5.6: Region (1)- The part $[1, \rho_2]$ of $[1, \infty)$ is admissible.

We carry out similar kind of analysis for the quadratic polynomial $F(S)$.

As $\varepsilon < 0$, the expression (4.8) for τ_S is transformed into

$$\frac{1}{2}\left(\frac{1}{\sqrt{-\varepsilon}}\int_{-1}^{1}\frac{dS}{\sqrt{(1-S^2)(S-S_1)(S-S_2)}}\right), \tag{5.20}$$

where $S_1 > 1$ and $S_2 > 1$ are the roots of the polynomial $F(S)$ given by:

$$S_1 = \frac{2\beta-\sqrt{(2\beta)^2-4A\varepsilon}}{-2\varepsilon}, \quad S_2 = \frac{2\beta+\sqrt{(2\beta)^2-4A\varepsilon}}{-2\varepsilon}.$$

Evaluating (5.20) in Maple software, we obtain

$$\tau_S = \frac{2K\left(\sqrt{\frac{2(S_2 - S_1)}{(S_2+1)(1-S_1)}}\right)}{\sqrt{-\varepsilon}\sqrt{(S_2+1)(1-S_1)}}. \tag{5.21}$$

We have the following scheme, showing the position of the roots S_1 and S_2, which corresponds to the region (V) in Figure 4.1.

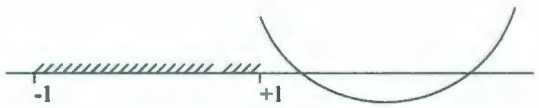

Figure 5.7: Region (V)- The whole interval $[-1, 1]$ for S is admissible.

The intersection of the two regions which we got from the above analysis is the region (V)(1) in the combined plot in Figure 4.20. Hence a range of admissible (A, ε) values: $A \in (-2, -\beta)$ and $\varepsilon \in (-\beta, 0)$.

Let us fix the value of $\varepsilon = -0.0901$ (a random choice within the admissible interval $(-0.1, 0)$). Picking specific values of A within the admissible range $(-2, -0.1)$ and substituting into (5.18) and (5.20), we get different values of half periods $\tau_\rho(A, \varepsilon)$ and $\tau_S(A, \varepsilon)$ displayed in Table 5.2.

Table 5.2: Different values of half periods τ_ρ, τ_S for $\varepsilon = -0.0901$

A	τ_S	τ_ρ
-0.100	1.547	1.092
-0.200	3.663	0.943
-0.300	2.856	0.956
-0.350	2.625	0.964
-0.380	2.513	0.968
-0.387	2.489	0.636
-0.500	2.182	0.968
-0.750	1.782	1.034

We derive the formulas for the phase shifts ϕ_S and ϕ_ρ in terms of A, ε based on the fact that the initial value of ρ_0 is 1:

$$\begin{aligned}\phi_\tau \tau_\rho &= \int_0^{\phi_\tau \tau_\rho} d\tau \\ &= \frac{1}{2}\int_1^{\rho_2} \frac{d\rho}{\sqrt{(\rho^2-1)(\varepsilon\rho^2+2\rho+A))}}.\end{aligned}$$

Therefore the phase shift ϕ_τ is

$$\phi_\tau = \frac{1}{2\tau_\rho}\int_1^{\rho_2} \frac{d\rho}{\sqrt{(\rho^2-1)(\varepsilon\rho^2+2\rho+A))}}. \tag{5.22}$$

In a similar manner, since $S_0 = 0$, the phase shift ϕ_S is given by

$$\phi_S = \frac{1}{2\tau_S}\int_{-1}^{0} \frac{dS}{\sqrt{(1-S^2)(-\varepsilon S^2-2\beta S-A))}}. \tag{5.23}$$

Table 5.3 displays different values of the phase shifts for varying values of A.

Table 5.3: Different values of the phase shifts ϕ_ρ, ϕ_S for $\varepsilon = -0.0901$

A	ϕ_S	ϕ_ρ
−0.100	0.469	0.619
−0.200	0.360	0.664
−0.300	0.406	0.631
−0.350	0.419	0.657
−0.380	0.425	0.656
−0.387	0.426	0.656
−0.500	0.442	0.650
−0.750	0.460	0.637

Suppose we want to make the planet hit the right star after 3 full half periods for $\rho(\tau)$ and 1 full half period for $S(\tau)$.

We substitute the values of $N_\rho = 3$ and $N_S = 1$ in the expressions (5.14) and (5.15). The required value of A is chosen in such a way that $\tau_{total1} = \tau_{total2}$. Here

both sides depend on A and we have an equation to solve for A. It involves elliptic integrals and we find an approximate solution using Tables 5.2–5.4.

Table 5.4 displays the corresponding values of τ_{total1} and τ_{total2} for different values of A and for fixed $\varepsilon = -0.0901$. We denote the difference between the total time periods by

$$\Delta\tau = \tau_{total2} - \tau_{total1}. \tag{5.24}$$

Our goal is to minimize $|\Delta\tau|$ numerically.

Table 5.4: Total elapsed time for $N_\rho = 3$ and $N_S = 1$

A	τ_{total2}	τ_{total1}	$\Delta\tau$
-0.100	2.274	3.955	-1.680
-0.200	4.986	3.455	1.530
-0.300	4.017	3.501	0.515
-0.350	3.726	3.528	0.198
-0.380	3.582	3.541	0.041
-0.387	3.551	3.546	0.005
-0.500	3.147	3.606	-0.458
-0.750	2.603	3.761	-1.157

Among the values of A presented in the Table 5.4 the one that minimizes $|\Delta\tau|$ is $A = -0.387$.

Substituting $\varepsilon = -0.0901$ in (5.9) we get

$$v \approx 1.151. \tag{5.25}$$

Substituting $A = -0.387$ and $\varepsilon = -0.0901$ in (5.11) we obtain

$$\psi \approx 0.393. \tag{5.26}$$

Hence the possible initial values for the particle to hit the right star are

$$v_0 \approx 1.151, \quad \psi \approx 0.393. \tag{5.27}$$

We simulated the motion numerically by choosing the above values of v_0 and ψ in the Matlab program (Appendix B). In Figures 5.8 and 5.9 the coordinates (x, y) are denoted as $(X1, X2)$.

Figure 5.8 displays the trajectory of the particle around the two fixed masses with $(x_0, y_0) = (0, 1)$, $v_0 = 1.15$, $\psi = 0.393$. It has been produced without the collision condition in the program. One can notice that particle continues its motion after narrowly escaping the collision with the right star (because of approximate values of initial data), almost backtracking the trajectory.

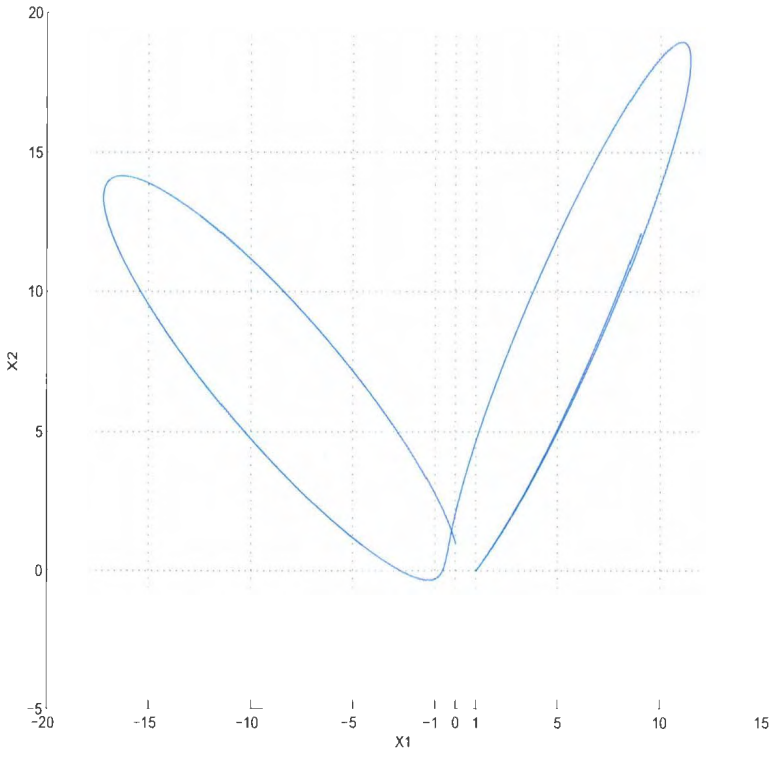

Figure 5.8: Trajectory of a particle narrowly escaping collision with the right mass

Figure 5.9 shows the trajectory of the particle colliding with the right fixed mass under the collision condition implemented in the Matlab program (Appendix B). It is assumed that the collision occurs if the distance between the particle and the right fixed mass is $\leq 10^{-6}$. There is no backtracking of its trajectory.

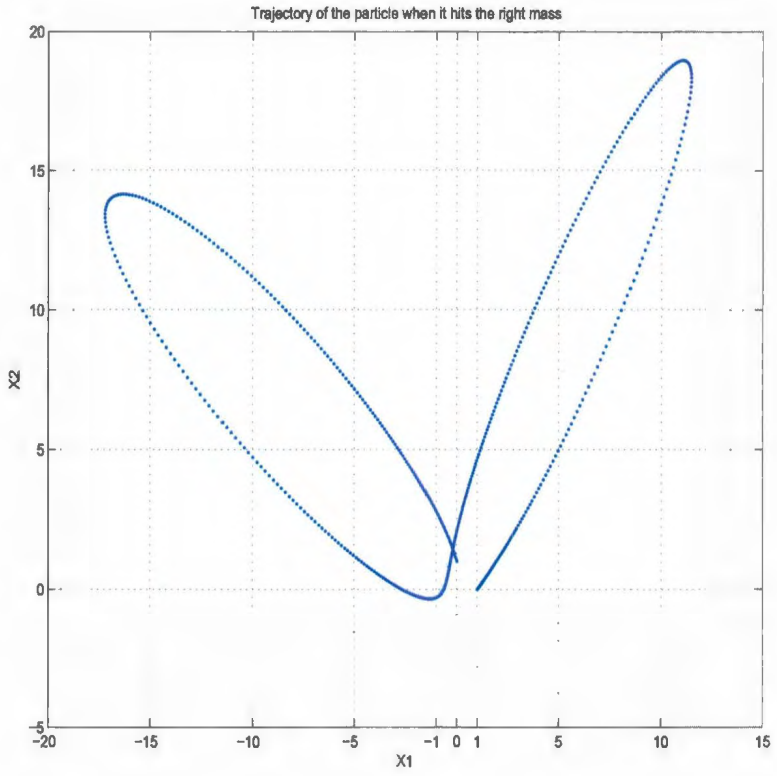

Figure 5.9: Trajectory of a particle colliding with the right fixed mass

Let us study the situation when the planet hits the left star. Figure 5.10 is a sample graph of the periodic function $\rho(\tau)$ and Figure 5.11 is a sample graph of the periodic function $S(\tau)$.

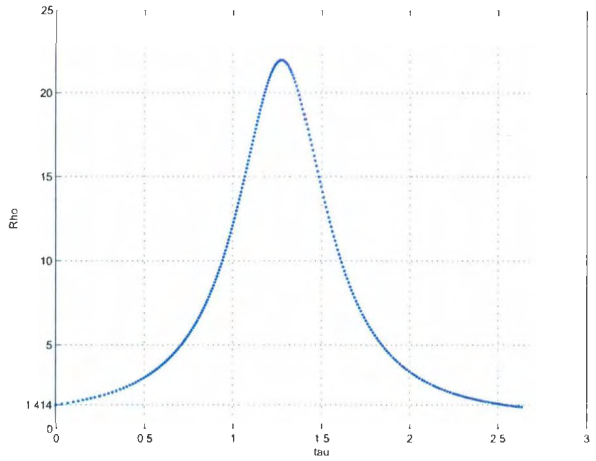

Figure 5.10: Plot of $\rho(\tau)$ showing 1 complete half period.

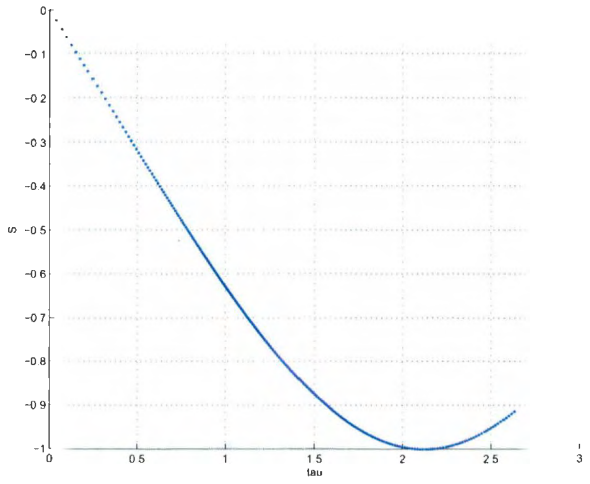

Figure 5.11: Plot of $S(\tau)$ showing incomplete half period

Let us fix the value of $\varepsilon = -0.0901$ as before.

Table 5.5 displays different values of A and the half periods τ_S and τ_ρ; while Table 5.6 displays different values of phase shifts for the same values of A.

Table 5.5: Different values of half periods τ_ρ, τ_S for $\varepsilon = -0.0901$

A	τ_S	τ_ρ
−0.110	16.324	0.930
−0.120	6.683	0.932
−0.130	5.621	0.933
−0.140	5.048	0.934
−0.150	4.662	0.936

Table 5.6: Different values of phase shifts ϕ_ρ, ϕ_S for $\varepsilon = -0.0901$

A	ϕ_S	ϕ_ρ
−0.110	0.095	0.667
−0.120	0.227	0.667
−0.130	0.265	0.666
−0.140	0.289	0.666
−0.150	0.307	0.665

Suppose we want to make the planet hit the left star after 1 full half period for $\rho(\tau)$ and 0 full half period for $S(\tau)$. Then $N_\rho = 1$ and $N_S = 0$. Substituting these values in the expressions (5.14) and (5.15), we produce the required value of A in such a way that (5.24) is minimized numerically.

Table 5.8 displays different values of τ_{total1}, τ_{total2} for different values of A and for the fixed $\varepsilon = -0.0901$.

The ranges of A values presented in tables 5.2–5.4, on the one hand, and in tables 5.5–5.7, on the other hand, are different because only the values close to the solution of equation (5.16) in the two different cases are included.

Table 5.7: Total elapsed time for $N_\rho = 1$ and $N_S = 0$

A	τ_{total1}	τ_{total2}	$\Delta\tau$
-0.110	1.555	1.552	0.003
-0.120	1.522	1.553	-0.031
-0.130	1.491	1.555	-0.064
-0.140	1.462	1.557	-0.094
-0.150	1.435	1.559	-0.123

We use the same criterion, i.e. to minimize $|\Delta\tau|$, to find the best approximation for A. Among the values of A presented in the Table 5.7, the one that minimizes $|\Delta\tau|$ is $A = -0.110$.

Substituting $\varepsilon = -0.0901$ in (5.9) we get

$$v_0 \approx 1.151. \tag{5.28}$$

Substituting $A = -0.110$ and $\varepsilon = -0.0901$ in (5.11) we obtain

$$\psi \approx 0.206. \tag{5.29}$$

Hence the initial values for the particle to hit the left star are

$$v_0 \approx 1.151, \quad \psi \approx 0.206. \tag{5.30}$$

Figure 5.12 displays the trajectory of the particle around the two fixed masses with $(x_0, y_0) = (0, 1)$, $v_0 = 1.15$, $\psi = 0.206$. It has been produced without the collision condition. One can notice that the particle continues its motion after narrowly escaping the collision with the left star (because of approximate values of initial data), almost backtracking its trajectory.

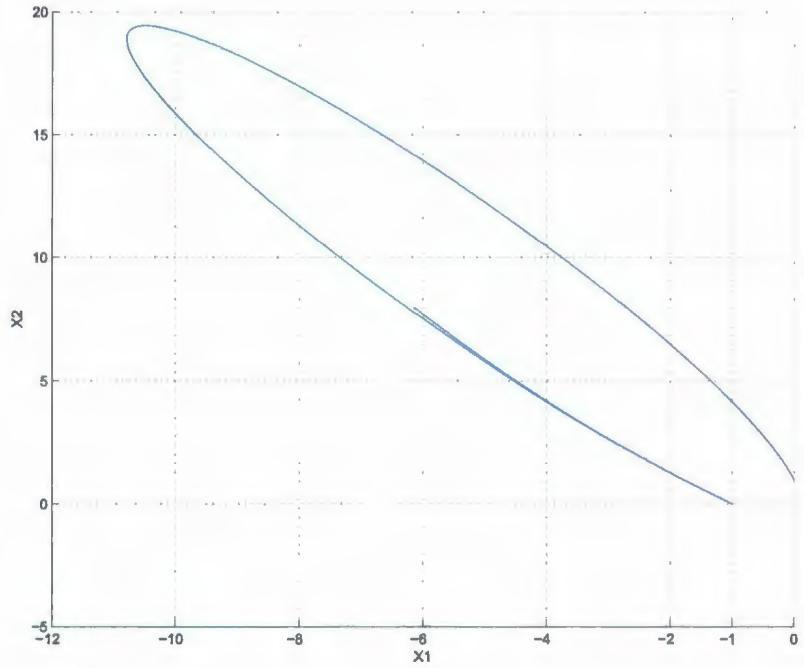

Figure 5.12: Trajectory of a particle around the two fixed masses narrowly escaping the collision with the left fixed mass

Figure 5.13 shows the trajectory of the particle colliding with the left fixed mass under the collision condition implemented in the Matlab program (Appendix C). It is assumed that the collision occurs if the distance between the particle and the left fixed mass is $\leq 10^{-6}$; the actual minimum distance turned out to be 10^{-8}. There is no backtracking of the trajectory.

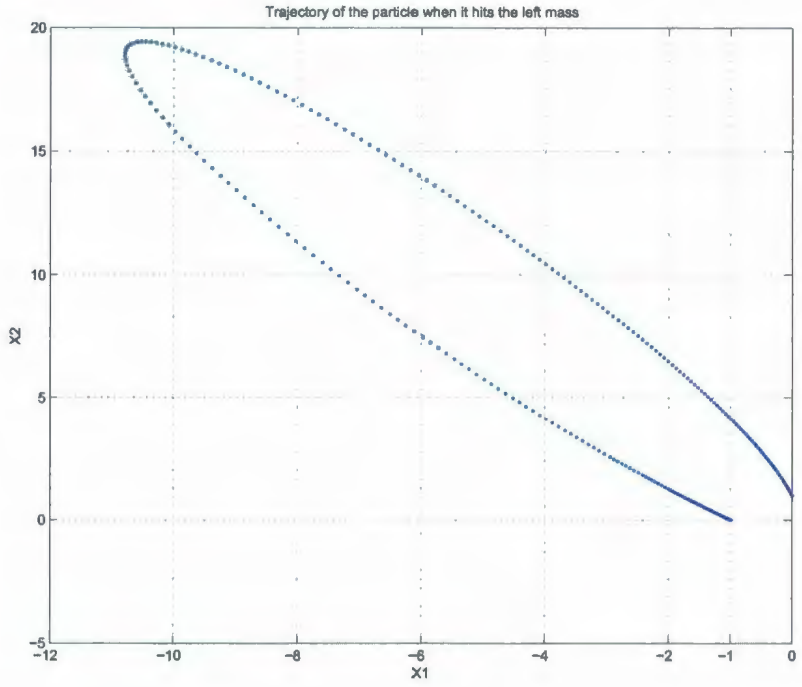

Figure 5.13: Trajectory of a particle colliding with the left fixed mass

Chapter 6

Comparison of regular and chaotic motion

6.1 The method of Poincare section

The Poincare section of a phase space is used to simplify the geometric description of the dynamics by reducing the dimension of the phase space. In general, this technique is used to represent a continuous trajectory in an N-dimensional space by its trace on an $(N-1)$-dimensional space. This is done by setting one of the phase elements to be a constant.

In a Hamiltonian system with two degrees of freedom the motion is confined to a 3-D energy surface. If the Hamiltonian system is integrable, then the motion occurs in a 2-D subspace of the energy surface, which is a torus if the motion is bounded.

We denote $(x, y) = (x_1, x_2)$ and the components of the velocity vector when it crosses the y-axis are denoted by (v_1, v_2).

Suppose the Hamiltonian system is determined by the Hamiltonian $H(x_1, x_2, p_1, p_2)$. The Hamiltonian function (energy) is an integral of motion. Any trajectory sits on an energy hypersurface $H(x_1, x_2, p_1, p_2) = E$, which is three dimensional in the four dimensional phase space. It never enters other level surfaces of the energy integral. So the dimension of the space where the dynamics occurs is reduced by 1 from 4-D

to 3-D. The Poincare section technique allows one to reduce the dimension of the dynamical space further, from 3-D to 2-D. For this purpose we use a 3-D hyperplane in the original 4-D phase space. Let it be $x_2 = 0$. Its intersection with the energy hypersurface is a 2-D surface. The component of velocity (v_1, v_2) at the moment of crossing are chosen the coordinates on it. If all the points of intersection of the trajectories with the section plane lie on a curve, then it conveys the existence of two integrals. If the points of intersection of the trajectories with the section plane fill up an area, then it conveys the existence of only one integral, which is energy.

6.2 Poincare section for our model

In this section we present some numerical results that show the integrability of the our model which we discussed in the previous chapters.

The Matlab program (see Appendix D) is written so that whenever the trajectory crosses from positive values of y to negative values of y (i.e. crosses the x-axis in the downward direction), the point at which the trajectory crossed is plotted in the Poincare section. A point is not shown in the Poincare section if the trajectory crosses from negative y values to positive y values. Figure 6.1 displays the projection of a trajectory onto the (x, y) plane and Figure 6.2 displays the corresponding numerical Poincare section.

In Figure 6.2 the curve is not a perfect one. The reason is the accumulation of numerical errors due to very large integration time.

We observe that the points of intersection of the trajectories with the section plane lie on a curve in the Poincare section in Figure 6.2. This tells us that there is an second integral of motion for our dynamical system. All the above plots of Poincare section were obtained by running the Matlab code included in Appendix D.

Figures 6.3, 6.4 display the projection of a trajectory of the particle confined between two ellipses and the corresponding Poincare section. The particle is initially placed at position $(x_0, y_0) = (0, 3)$.

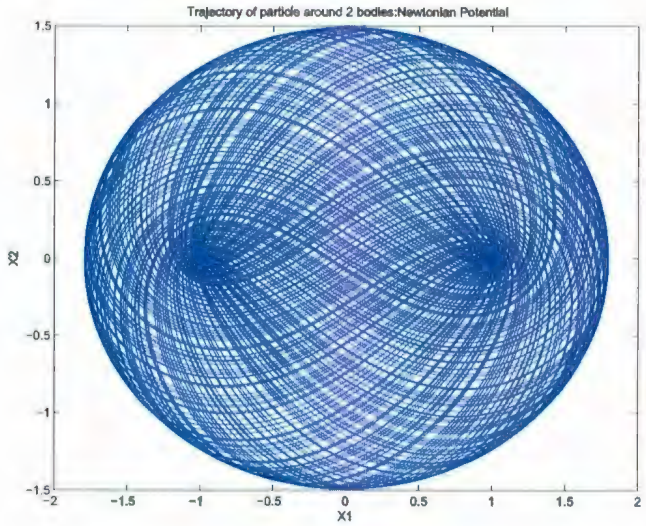

Figure 6.1: Trajectory of particle with initial values $(v, \psi) = (0.75, \frac{\pi}{3})$, corresponding $(A, \varepsilon) = (-0.843, -0.851)$, integration time=1200

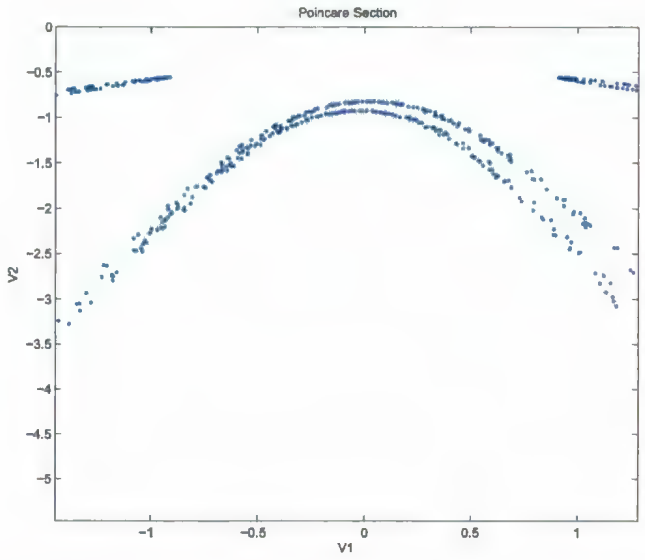

Figure 6.2: Poincare section with initial values $(v, \psi) = (0.75, \frac{\pi}{3})$, corresponding $(A, \varepsilon) = (-0.843, -0.851)$, integration time=30000

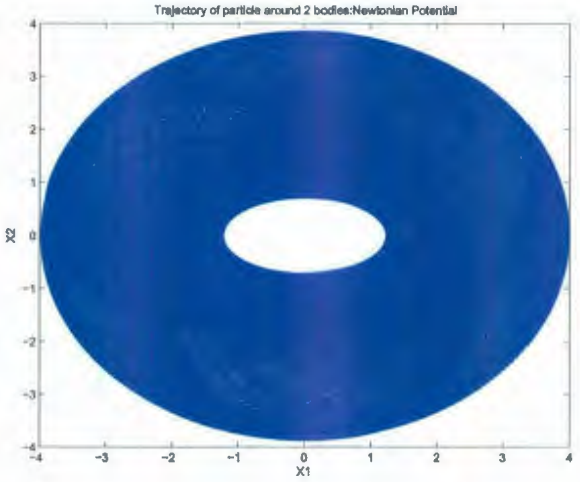

Figure 6.3: Trajectory of particle with initial values $(v, \psi) = (0.5, \frac{\pi}{3})$, corresponding $(A, \varepsilon) = (-0.375, -1.164)$, integration time=30000

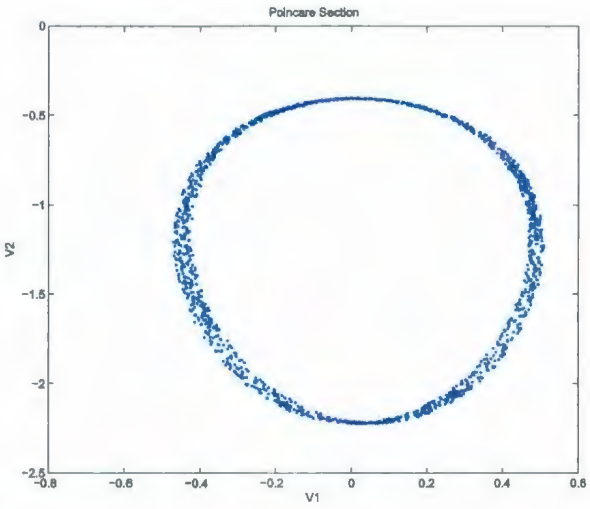

Figure 6.4: Poincare section with initial values $(v, \psi) = (0.5, \frac{\pi}{3})$, corresponding $(A, \varepsilon) = (-0.375, -1.164)$, integration time=30000

Figures 6.5 and 6.6 display the trajectories of the particle colliding the right fixed mass and the corresponding Poincare section. (Figure 6.5 is identical to Figure 5.9)

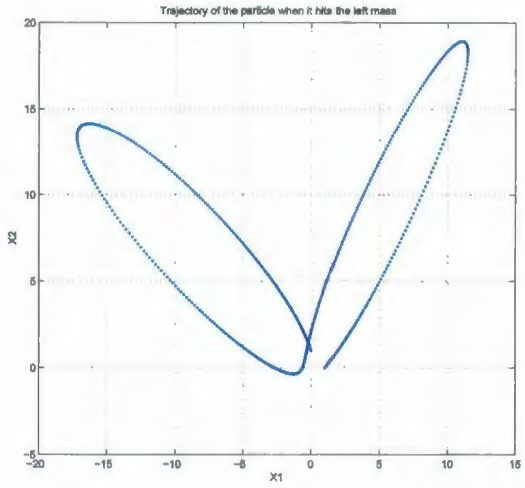

Figure 6.5: Trajectory of particle with initial values $(v, \psi) = (1.1507, 0.393)$, corresponding $(A, \varepsilon) = (-0.387, -0.0901)$, integration time=500

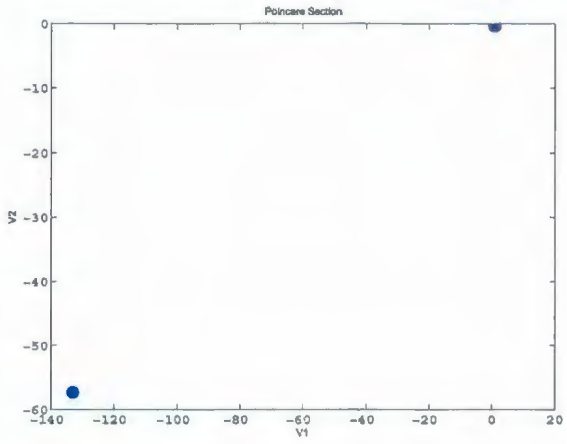

Figure 6.6: Poincare section with initial values $(v, \psi) = (1.1507, 0.393)$, corresponding $(A, \varepsilon) = (-0.387, -0.0901)$, integration time=500

In Figure 6.6, we observe only two points in the Poincare section, one near the upper right corner and another near the bottom left corner.

From Figure 6.5 we observe that the trajectory of the particle crosses the x-axis from the left side of the left fixed mass; the corresponding point is plotted on the Poincare section near upper right corner and the velocity is small. The point where the trajectory crosses the x-axis in the upward direction from the right side of the left fixed mass is not displayed on the Poincare section.

The trajectory then crosses the x-axis from the left side of the left fixed mass before colliding with it; the corresponding point is plotted on the Poincare section near bottom left corner and the velocity is large. The above plots were obtained by running the Matlab code in Appendix B, D.

Figures 6.7 and 6.8 display the trajectory of the particle colliding the left fixed mass and the corresponding Poincare section.

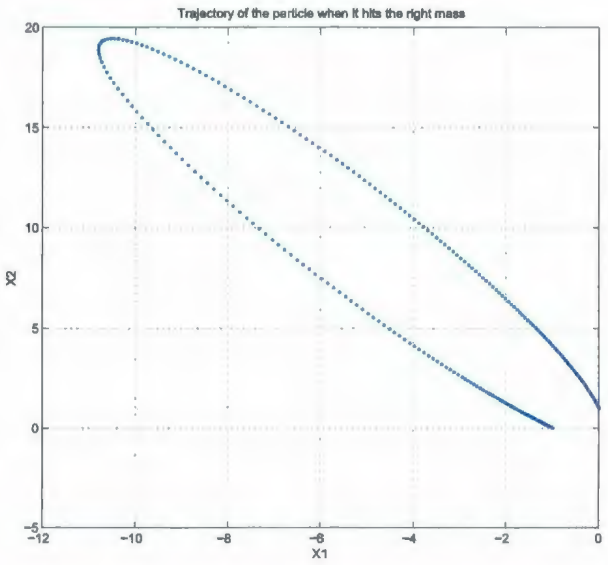

Figure 6.7: Trajectory of particle with initial values $(v, \psi) = (1.1507, 0.206)$, corresponding $(A, \varepsilon) = (-0.110, -0.0901)$, integration time=250

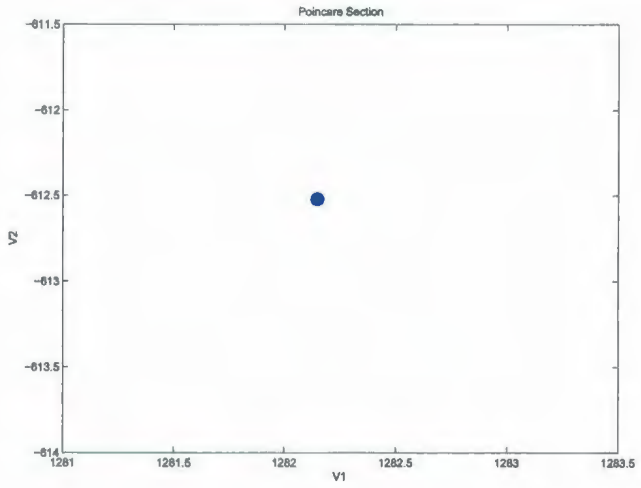

Figure 6.8: Poincare section with initial values $(v, \psi) = (1.1507, 0.206)$, corresponding $(A, \varepsilon) = (-0.110, -0.0901)$, integration time=250

In Figure 6.7 we observe that the trajectory of the particle crosses the x-axis from the left side of the left fixed mass (shortly before hitting it); the corresponding point is plotted on the Poincare section in Figure 6.8, where it is the only point located in the center of the plot. These plots were obtained by running Matlab code in Appendix C, D.

6.3 The model with logarithmic potential

In this section we present some numerical results that demonstrates the non integrability of the given model with Logarithmic potential.

We now introduce another model to compare its behaviour with the model we have dealt with in the previous chapters. The force of attraction in this model obeys the inverse first power law. The corresponding potential function is logarithmic.

In this section we refer to the main model as the one with "Newtonian potential" and the new model as the one with "logarithmic potential".

The potential energy per unit mass in the gravitational field of the two fixed masses at the point $P(x, y)$ in the new model is given by

$$U(x, y) = -(m_1 \ln r_1 + m_2 \ln r_2). \tag{6.1}$$

The new Hamiltonian function is

$$H(x, y, p_x, p_y) = \frac{1}{2}(p_x^2 + p_y^2) - (m_1 \ln r_1 + m_2 \ln r_2).$$

Figures (6.9) and (6.10) display a sample trajectory of a particle around the two fixed masses in the model with logarithmic potential and the corresponding numerical Poincare section.

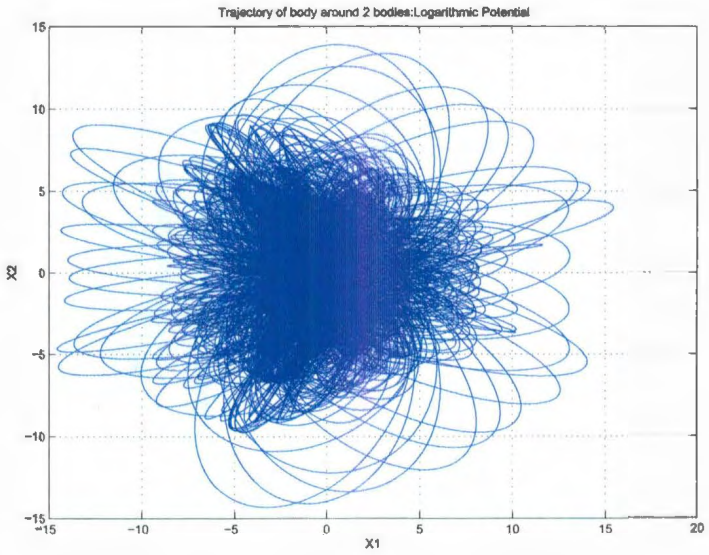

Figure 6.9: Trajectory of particle with initial values $(v, \psi) = (0.25, \frac{\pi}{3})$, corresponding $(A, \varepsilon) = (-0.093, -1.351)$, integration time=50000

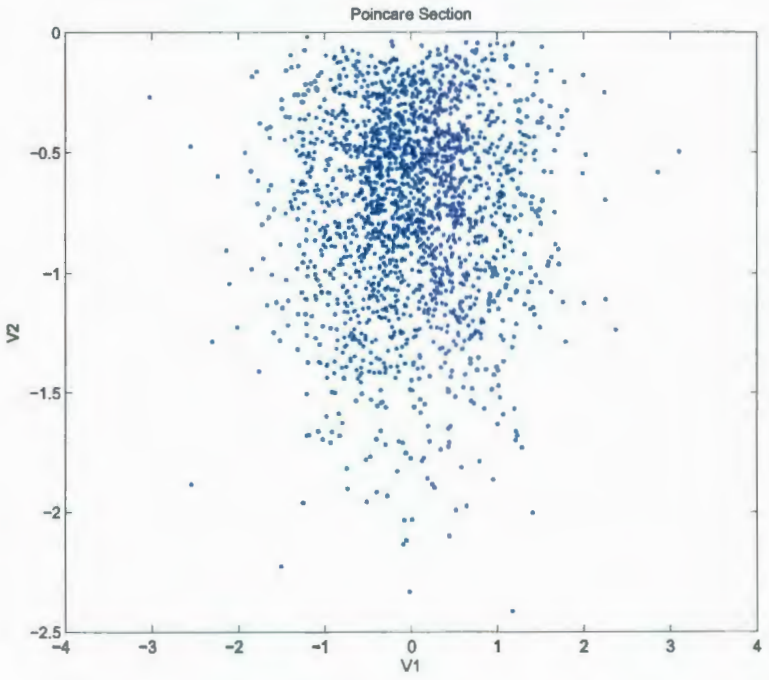

Figure 6.10: Poincare section with initial values $(v, \psi) = (0.25, \frac{\pi}{3})$, corresponding $(A, \varepsilon) = (-0.093, -1.351)$, integration time=50000

In Figure 6.9 it is seen that the trajectory of the particle is not confined to a 2-D torus, while it dwells on 3-D hypersurface where energy is constant. We observe that the points of intersection of the trajectories with the section plane fill up a region in the Poincare section in Figure 6.10 due to the chaotic behavior observed in Figure 6.9. This tells us that there is no second integral of motion for the Hamiltonian with logarithmic potential.

Conclusion

We have presented the study of the two fixed centers problem restricted to a two dimensional case. To do so, we used the Hamiltonian approach. First, applying the Jacobi's method of generating function, we transformed the Hamiltonian system to elliptic coordinates. Using Liouville's theorem we derived two integrals of motion besides the energy integral. The independent Hamiltonian systems are then integrated to get an analytical solution in terms of elliptic integrals.

We analyzed the roots of quadratic polynomials that control the behaviour of elliptic integrals. Then we presented various bounded and unbounded cases of motion and classified different types of trajectories accordingly.

Two applications of the theory were studied. We defined the first and the second escape velocities. The formulae for both the escape velocities were derived and numerical results were presented. In the second application, given initial position of the particle, we calculated the initial velocity and the angle at which the particle should start so that it hits either the left fixed mass or the right fixed mass.

Theoretical predictions were also compared with numerical results by studying the Poincare section. We first defined the Poincare section and described the method of reducing the dimension of the phase space. Then we considered logarithmic potential, corresponding to the attraction law of inverse first powers.We studied the difference between the integrable system with Newtonian potential and a non-integrable system with logarithmic potential through the Poincare section technique.

Appendix A

Matlab Code for numerical integration of ODE system

```
% This code is used for integrating the ODE system and plots the
% trajectory of the particle around the two fixed centers.

%-----------------------------------------------------------------

% This is the main function: Save this m-file with the
% file name threebodydesignmain.m

clc;
close all;
threebodydesignhandle = @threebodydesign;


RelTol = input('Enter the relative tolerance level: ');
options = odeset('RelTol',RelTol);
```

```
V0 = input('Enter the speed of the particle: ');
Tmax = input('Enter number of iterations: ');
l = input('Enter the position of the particle: ');
theta = input('Enter the angle at which the particle starts: ');

x = -V0*sin(psi);
y = V0*cos(psi);

[T,Y] = ode45(@threebodydesign,[0 Tmax],[0;l;x;y],options);

figure(1);
plot(Y(:,1),Y(:,2))
xlabel('X1');
ylabel('X2');

title('Trajectory of particle around 2 bodies:Newtonian Potential');

%-----------------------------------------------------------------

% This is the sub function: Save this m-file as threebodydesign.m
% in the same folder where main file is saved.

function Z = threebodydesign(t,X)

G = 1;
m1 = 0.45;
m2 = 0.55;
L = +1;
beta = m2-m1;
```

```
r1 = ((X(1)-L)^2+X(2)^2)^(3/2);
r2 = ((X(1)+L)^2+X(2)^2)^(3/2);

A=G*[-(m1*(X(1)-L)/r1+m2*(X(1)+L)/r2);-((m1*X(2))/r1+(m2*X(2))/r2)];

Z=[X(3);X(4);A(1);A(2)];
```

Appendix B

Matlab Code for particle colliding with right fixed mass

```
% This code simulates 2 fixed center problem. Two bodies
% with masses m1 and m2 are fixed at (1,0) and (-1,0)
% respectively. A particle P is placed at (0,1). This
% code simulates the particle colliding with the right
% fixed  mass for a given initial velocity and the angle
% at which the particle starts from its initial position
% (the parameters which we calculated from the theory).

% USER:
% The user should input the parameters initial velocity
% of the particle and the angle at which the particle
% starts from its initial position as calculated from
% the theory. The parameters change for the left fixed
% mass and for the right fixed mass.

% OUTPUT:
```

```
% The output displays the trajectory of the particle before
% it collides with the right fixed mass (the program ends when
% the particle is close to the right fixed mass)


% This is the sub function: Save this m-file separately
% with the file name threebodydesign.m

function Z = threebodydesign(t,X)

G = 1;
m1 = 0.45;
m2 = 0.55;
L = +1;
beta = m2-m1;

r1 = ((X(1)-L)^2+X(2)^2)^(3/2);
r2 = ((X(1)+L)^2+X(2)^2)^(3/2);

A=G*[-(m1*(X(1)-L)/r1+m2*(X(1)+L)/r2);-((m1*X(2))/r1+(m2*X(2))/r2)];

Z=[X(3);X(4);A(1);A(2)];


%-----------------------------------------------------------------

% This is the main function: Save this m-file separately
% with the file name threebodydesignmain.m
```

```
clc;
close all;

threebodydesignhandle = @threebodydesign;

RelTol = input('Enter the relative tolerance level: ');
options = odeset('RelTol',RelTol);

V0 = input('Enter the velocity of the particle: ');
Tmax = input('Enter number of iterations: ');
l = 1;
psi = input('Enter the angle: ');

x = -V0*sin(psi);
y = V0*cos(psi);

[T,Y]=ode45(@threebodydesign,[0 Tmax],[0;l;x;y],options);


% This part of the code is for displaying the minimum
% value (minimum distance at which the particle is to
% the right fixed mass).

q = 1;

while(q < k(1))
    q;
    temp1(q) = sqrt((Y(q,1)+1)^2+Y(q,2)^2);
```

```
    q = q + 1;
end

b = min(temp1);
display(['Min.distance particle close to right mass:',num2str(b)]);


% This code plots the trajectory of the particle when it
% hits right fixed mass (The program ends when the particle
% is at a minimum distance from the right fixed mass).

p = 1;

while(p < k(1))

    p;
    temp = sqrt((Y(p,1)+1)^2+Y(p,2)^2);
    hold on
    if temp > b
        p;
        figure(1);
        plot(Y(p,1),Y(p,2),'.')
        xlabel('X1');
        ylabel('X2');
        grid on
        name = strcat(['Collision of particle with right mass)']);
        title(name);
     end
    if temp == b
```

```
        % The program ends at the minimum distance.
        display(['The program ended at:',num2str(temp)])
        break
    end
 hold off
 p = p+1;
end


%-------------------------------------------------------
```

Appendix C

Matlab Code for particle colliding with left fixed mass

```
% This code simulates 2 fixed center problem. Two bodies
% with masses m1 and m2 are fixed at (1,0) and (-1,0)
% respectively. A particle P is placed at (0,1). This
% code simulates the particle colliding with the left
% fixed  mass for a given initial velocity and the angle
% at which the particle starts from its initial position
% (the parameters which we calculated from the theory).

% USER:
% The user should input the parameters initial velocity
% of the particle and the angle at which the particle
% starts from its initial position as calculated from
% the theory. The parameters change for the left fixed
% mass and for the right fixed mass.

% OUTPUT:
```

```
% The output displays the trajectory of the particle before
% it collides with the left fixed mass (the program ends
% when the particle is close to the left fixed mass)


% This is the sub function: Save this m-file separately
% with the file name threebodydesign.m

function Z = threebodydesign(t,X)

G = 1;
m1 = 0.45;
m2 = 0.55;
L = +1;
beta = m2-m1;

r1 = ((X(1)-L)^2+X(2)^2)^(3/2);
r2 = ((X(1)+L)^2+X(2)^2)^(3/2);

A=G*[-(m1*(X(1)-L)/r1+m2*(X(1)+L)/r2);-((m1*X(2))/r1+(m2*X(2))/r2)];

Z=[X(3);X(4);A(1);A(2)];


%-----------------------------------------------------------------

% This is the main function: Save this m-file separately
% with the file name threebodydesignmain.m
```

```
clc;
close all;

threebodydesignhandle = @threebodydesign;

RelTol = input('Enter the relative tolerance level: ');
options = odeset('RelTol',RelTol);

V0 = input('Enter the velocity of the particle: ');
Tmax = input('Enter number of iterations: ');
l = 1;
psi = input('Enter the angle: ');

x = -V0*sin(psi);
y = V0*cos(psi);

[T,Y]=ode45(@threebodydesign,[0 Tmax],[0;l;x;y],options);


% This part of the code is for displaying the minimum
% value (minimum distance at which the particle is to
% the left fixed mass).

q = 1;

while(q < k(1))
    q;
    temp1(q) = sqrt((Y(q,1)-1)^2+Y(q,2)^2);
```

```
    q = q + 1;
end

b = min(temp1);
display(['Min.distance particle close to left mass:',num2str(b)]);


% This code plots the trajectory of the particle when it
% hits left fixed mass (The program ends when the particle
% is at a minimum distance from the left fixed mass).

p = 1;

while(p < k(1))

    p;
    temp = sqrt((Y(p,1)-1)^2+Y(p,2)^2);
    hold on
    if temp > b
        p;
        figure(1);
        plot(Y(p,1),Y(p,2),'.')
        xlabel('X1');
        ylabel('X2');
        grid on
        name = strcat(['Collision of particle with left mass)']);
        title(name);
     end
    if temp == b
```

```
        % The program ends at the minimum distance.
        display(['The program ended at:',num2str(temp)])
        break
    end
 hold off
 p = p+1;
end

%-------------------------------------------------------
```

Appendix D

Matlab code for plotting the Poincare section

```
% This code plots the Poincare section.
%-----------------------------------------------------------------
% This is the main function: Save this m-file with the
% file name threebodydesignmain.m

clc;
close all;
threebodydesignhandle = @threebodydesign;

RelTol = input('Enter the relative tolerance level: ');
options = odeset('RelTol',RelTol);

V0 = input('Enter the speed of the particle: ');
Tmax = input('Enter number of iterations: ');
l = 1;
psi = input('Enter the angle at which the particle starts: ');
```

```
x = -V0*sin(psi);
y = V0*cos(psi);

[T,Y] = ode45(@threebodydesign,[0 Tmax],[0;l;x;y],options);

j = 1;
k = size([T,Y]);
while(j < k(1))

    j;
    hold on
    if (Y(j,2) > 0 && Y(j+1,2) < 0)
        j;
        figure(1);
        plot(Y(j,3),Y(j,4),'.')
        xlabel('V1');
        ylabel('V2');
        title('Poincare Section')
    end

  hold off
  j = j+1;
end

%-----------------------------------------------------------------

% This is the sub function: Save this m-file as threebodydesign.m
% in the same folder where main file is saved.
```

```
function Z = threebodydesign(t,X)

G = 1;
m1 = 0.45;
m2 = 0.55;
L = +1;
beta = m2-m1;

r1 = ((X(1)-L)^2+X(2)^2)^(3/2);
r2 = ((X(1)+L)^2+X(2)^2)^(3/2);

A=G*[-(m1*(X(1)-L)/r1+m2*(X(1)+L)/r2);-((m1*X(2))/r1+(m2*X(2))/r2)];

Z=[X(3);X(4);A(1);A(2)];
%-------------------------------------------------------------------
```

Bibliography

[1] Aksenov, E.P., Grebennikov, E.A., and Demin, V.G., General solution to the problem of motion of a satellite in the normal field of attraction of the Earth, *Iskusstvennye Sputniki Zemli* (Artificial satellites of the Earth), **8** (1961), 64–72.

[2] Beletskii, V. V., *Essays on the Motion of Celestial Bodies*, Birkhäuser, 2001.

[3] Carretero-González, R., Núñez-Yépez, H.N., and Salas-Brito, A.L., Regular and chaotic behavior in an extensible pendulum, *Eur. J. Physics*, **15** (1994), 139–148.

[4] Charlier, C.L., *Die Mechanik des Himmels*, Leipzig, Verlag von Veit, 1902.

[5] Contopoulos, G. and Papadaki, H., Newtonian and Relativistic Periodic Orbits around two fixed black holes, *Cel. Mech. Dyn. Astron.*, **55** (1993), 47–85.

[6] Deprit, A. Le probleme des deux centers fixes, *Bull. Soc. Math. Belg.*, **142** (1962), 12–45.

[7] Euler, L. De motu coproris ad duo centra virium fixa attracti, *Nov. Comm. Acad. Sci. Imp. Petrop*, **10** (1766), 207–242.

[8] Euler, L. De motu coproris ad duo centra virium fixa attracti, *Nov. Comm. Acad. Sci. Imp. Petrop*, **11** (1767), 152–184.

[9] Euler, L. Problème. Un corps étant attiré en raison réciproque quarrée des distances vers vers deux points fixes donnés, trouver les cas ou la courbe décrite par ce corps sera algébrique, *Mémoires Berlin de l'Acad des Sci. de*, **2** (1767), 228–249.

[10] Goldstein, H., *Classical Mechanics*, 2nd ed., Addison-Wesley, 1980.

[11] Erikson, H.A. and Hill, E.L., A note on the one electron states of diatomic molecules, *Phys. Rev.*, **75:1** (1949), 29–31.

[12] Robert, H.C., *Chaos and Nonlinear Dynamics*, Oxford University Press, 1994.

[13] Jacobi, C.G.J. *Vorlesungen über Dynamik*, Collected works, 2nd ed., Bd. VIII, Chelsea Publishing Company, 1969.

[14] Neissen, K.F., Zür Quantentheorie des Wasserstoffmolekulions, *Annalen der Physik*, **375:2** (1923), 129–134.

[15] Ó Mathúna, D. *Integrable Systems in Celestial Mechanics*, Birkhäuser, 2008.

[16] Pauli, W., Über das Modell Wasserstoffmolekulions, *Annalen der Physik*, **373:11** (1922), 177–240.

[17] Strand, M.P. and Reinhardt, W.P., Semiclassical quantization of the low lying electronic states of H_2^+, *J. Chem. Phys.*, **70:8** (1979), 3812–3827.

[18] Szebehely, V, *Theory of orbits—The restricted problem of three bodies*, Academic Press, 1967.

[19] Tallquist, H.J. Über die Bewegung eines Punktes welcher von zwei festen Zentren nach dem Newtonschen Gesetze angezogen wird, *Acta Soc. Sci. Fenn.*, A, **NS 1:5** (1927).

[20] Varvoglis, H., Vozikis, C.H., and Wodnar, K., The Two Fixed Centers: An Exceptional Integrable System, *Cel. Mech. Dyn. Astron.*, **88** (2004), 343–356.